Fall 2013

Modeling and control of nanoparticle bloodstream concentration for cancer therapies

Scarlett S. Bracey

MODELING AND CONTROL OF NANOPARTICLE BLOODSTREAM CONCENTRATION FOR CANCER THERAPIES

by

Scarlett S. Bracey, B.S., M.S., M.S.E.

A Dissertation Presented in Partial Fulfillment
of the Requirements for the Degree
Doctor of Philosophy

COLLEGE OF ENGINEERING AND SCIENCE
LOUISIANA TECH UNIVERSITY

November 2013

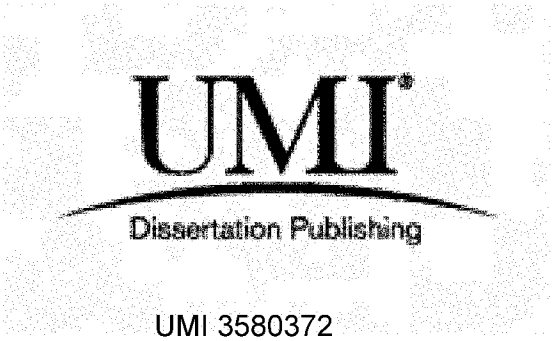

ProQuest LLC
789 East Eisenhower Parkway
P.O. Box 1346
Ann Arbor, MI 48106-1346

LOUISIANA TECH UNIVERSITY

THE GRADUATE SCHOOL

30 September 2013

Date

We hereby recommend that the dissertation prepared under our supervision by Scarlett S. Bracey, MS, MSE

entitled Modeling and Control of Nanoparticle Bloodstream Concentration for Cancer Therapies

be accepted in partial fulfillment of the requirements for the Degree of PhD Computational Analysis and Modeling

Supervisor of Dissertation Research

Head of Department

Mathematics

Department

Recommendation concurred in:

Advisory Committee

Approved:

Director of Graduate Studies

Approved:

Dean of the Graduate School

Dean of the College

GS Form 13a
(6/07)

ABSTRACT

Currently, the most commonly used treatments for cancerous tumors (chemotherapy, radiation, etc.) have almost no method of monitoring the administration of the treatment for adverse effects in real time. Without any real time feedback or control, treatment becomes a "guess and check" method with no way of predicting the effects of the drugs based on the actual bioavailability to the patient's body. One particular drug may be effective for one patient, yet provide no benefit to another. Doctors and scientists do not routinely attempt to quantifiably explain this discrepancy.

In this work, mathematical modeling and analysis techniques are joined together with experimentation to gain further insight into the challenges of nanoparticle uptake and retention in the bloodstream. Several models are presented here which predict both the uptake and retention phases of the experiment. There does exist a commonly accepted model of drug clearance in the pharmacokinetics community, and it is demonstrated here that this model provides an accurate reflection of reality, as observed in experiments, for delivery of gold-coated nanorods. This model is then utilized in a state space feedback control framework to regulate the nanoparticle concentration in the bloodstream. An equal time delay is also introduced in both the state and control input for the purpose of studying alternate dosing strategies. This study will aid in the prediction of the effects of the drugs in a patient's body, thus leading to better models for drug regimen and administration.

APPROVAL FOR SCHOLARLY DISSEMINATION

The author grants to the Prescott Memorial Library of Louisiana Tech University the right to reproduce, by appropriate methods, upon request, any or all portions of this Dissertation. It is understood that "proper request" consists of the agreement, on the part of the requesting party, that said reproduction is for his personal use and that subsequent reproduction will not occur without written approval of the author of this Dissertation. Further, any portions of the Dissertation used in books, papers, and other works must be appropriately referenced to this Dissertation.

Finally, the author of this Dissertation reserves the right to publish freely, in the literature, at any time, any or all portions of this Dissertation.

Author S. Bray

Date 31 Oct, 2013

DEDICATION

This dissertation is dedicated to my best friend Nicholas, our handsome son Russell Driller, and our beautiful daughter Vivien McKenzie.

TABLE OF CONTENTS

LIST OF TABLES

LIST OF FIGURES

ACKNOWLEDGMENTS

I first and foremost give praise to my God for this opportunity that He has blessed me with and for all of the people whom He has placed in my life so that I would be prepared for the challenges that has come along with it.

I would have never even been close to this point without the dedication of my research advisor Dr. Katie Evans. She has put her faith in me throughout this entire process and has given me no excuse to fail. I will thank my God every time I think of the role she has played in my life; and I pray that she always knows how grateful I am to her.

I am so grateful to my friends who conquered this path ahead of me. Dr. Lisa James and Dr. Krystal Corbett faced the challenges of the dissertation writing and defending and shared their knowledge with me every step of the way. They, along with so many other of my fellow students, helped make this experience one to be cherished instead of regretted. Also to my friends not going through the pains of graduate school, thank you for listening as I had nothing else to talk about for several years. Lindsey Crawford, Brenda Lofton, and Allison Milstead, your encouraging words and prayers at every step got me through some very rough points.

The constant prayer, patience, and discipline from my parents throughout my entire life has given me the strength and guidance I have needed along this journey. God chose you to be my parents, thank you for not taking that responsibility lightly.

And Kathy Nelson, my college mom, continued the work that my parents began with prayer and discipline. And also to Russell and Becky Bracey, you taught my husband to be the man that he is today and I can never thank you enough for that gift.

And of course, my husband Nicholas, stayed by side and pushed me forward the whole way through. Our children provided me with some great study buddies and I never could have done it without them.

CHAPTER 1

INTRODUCTION

Though cancer therapies can be effective, there is almost no way to predict the effect that a particular therapy will have on any one individual [34]. As current treatment dosages are largely determined by the weight of the subject, there is almost no way of predicting the efficacy or any adverse effects while the drug is being administered. Mathematical models and controls have been applied towards developing strategies which would determine when and how much of a drug to inject to produce a prolonged and effective therapeutic result [10], [11], [12], [23], [39]. However, the combination of mathematical models with real-time clinical data could assist in providing better quality control in dosing. Predictive models could further help in identifying adverse events prior to the onset of signs and symptoms.

In recent years, clinical studies have been carried out for measurements of the uptake and clearance of engineered gold nanoparticles in the tissues of dosed mice [18], [26], [27], [28], [29]. These devices are under consideration for a new therapy for cancerous tumors. Clinical trials in animals are currently underway to investigate the therapeutic bioavailability of nanoparticles used in the treatment of these tumors in a technique known as nanoparticle-assisted photothermal cancer therapy, such as in [26] and [27]. The research presented here investigates the development of mathematical

models to estimate in real-time the circulation parameters of models, from which we calculate the area-under-the-curve (AUC) and half-life towards a clinical application. These particular variables can be telling of the overall retention of the nanoparticles [17], [28], as will be discussed in Chapter 2.

In this dissertation, we present a framework for the least error models of the experiments that can be created in real time (that is, within the time of which the experiment is run). Many different modeling methods were considered for this work that dealt with separating the body into different compartments (i.e. the reticulo-endothelial system, the tumor, the lungs, etc.) [17], [20], [37], [38] and also those that dealt with only a single compartment (the entire body at once) [5], [9], [14], [15], [22]. It was decided, for this work, to model a single compartment. This is due to a lack of clinical data for accumulation in the tumor, clearance by the Reticulo Endothelial System, etc. Without this data is not possible to accurately model what is happening in the separate compartments of the body. Several different models are presented, each of which provides a best fit for different times in the experiments. We start with a rational function model which mimics models that were found in the literature that include both the uptake and retention phases [17]. We then show the exponential model in order to have a model which focuses strictly on the retention phase of the experiment. Also, in an effort to improve upon the skewed rational model, an absolute value model is presented. Finally, a piecewise function is presented which combines a certain desired shape for the injection phase of the experiment and the already found exponential best fit for the retention phase.

Upon completion of these models, statistical tests were employed to determine if the data were correlated enough to take averages without losing generality. The Spearman Ranked Correlation test was done on several different pairs of data sets to determine whether or not certain experimental variables were related. The Wilcoxon Signed Rank test was then performed to ensure that every value within each individual data set was statistically similar. We then averaged each model for each set of data and created confidence bounds and prediction intervals. These averaged models, or 'Master Mice', were calculated, along with the confidence and prediction intervals, so that, in future experiments, adverse reactions (such as allergic reactions or significant clearance rates) may be detected within the time of the experiment and changes in dosage rates can be made accordingly. The 'Master Mice' also provide appropriate data sets to test using the controllers that are discussed in Chapters 4 and 5.

A Linear Quadratic Regulator (LQR) tracking controller (as discussed in [7] and [4]) was then applied to the averaged models, or 'Master Mice'. This controller was implemented on a delay differential equation model and included a tracking feature to regulate the bloodstream nanoparticle concentration to a desired absorbance value (measured in OD). Currently, the controller is only applied to the exponential model as this is the most commonly referenced model in the literature. However, as a delay differential equation takes the history of the function into account, the injection phase of the piecewise model is included here. This controller is further analyzed by changing the amount of the initial injection in order to investigate the possibility of limiting the total amount of nanoparticles required experimentally. Dirac delta functions are then used in place of the continuous time controller to determine the

efficacy of a discrete amount of injections to control the absorbance level as opposed to the continuous injection used in the LQR controller. Finally, a Proportional Integral Derivative (PID) controller for a delay differential equation (similar to those discussed in [33]) is applied to the problem in an attempt to control not only the absorbance value (in OD) over time but the area under the curve as well.

The goal of this work is to be able to use the model and controller in real time during the injection and elimination phase of nanoparticle administration to a subject. The use in real time situations would provide feedback in case of adverse reaction or if the dose needs to be increased or decreased according to the subject's reaction. Ideally, the feedback controller would also be used during the experiment so that the optimal level of nanoparticles would circulate through the bloodstream for the maximum allowable time.

Chapter 2 contains background information of the experimental work that is has been done to obtain the data and also describes each of the least error models, along with the method that was employed to obtain the models. Chapter 3 describes the statistical tests that were run on the data and discusses what the results represent, along with a description of the average models with the corresponding confidence and prediction intervals. The control strategies and results are discussed in Chapters 4 and 5. Finally, in Chapter 6 we conclude with observations and future work.

CHAPTER 2

LEAST ERROR MODELS

2.1 Experimental Design

The objective of the pre-clinical experiment from which the data reported here was obtained was to investigate the pharmacokinetic properties of therapeutic gold nanorods. These 40-nm diameter gold nanorods were manufactured by Nanospectra Biosciences, Inc (NBI) (Houston, TX) and are used for the photothermal ablation of tumor cells [1], [32]. That is, the nanorods are first injected into the bloodstream; then, upon collection in the tumor, the nanorods are given laser treatment that causes them to heat to the point of killing the vasculature of the tumor, thus killing the tumor. They are used in the experiments from which the data is collected specifically with murine colon carcinomas. These tumors are grown on the flank of the mouse just beneath the skin until the tumor reaches the desired size. Once the tumor was the appropriate size, the nanorods were injected and circulation data was collected.

The data was collected by the O'Neal group in the Biomedical Engineering program at Louisiana Tech University in collaboration with NBI. The real-time blood concentration of the nanorods was monitored using a novel non-invasive optical device similar to a pulse oximeter [26], [27], [28]. This experimental pulse photometer,

also referred to as the 'NanoTracker', uses the technique of multi-wavelength photoplethysmography [1]. The NanoTracker measures the attenuation of near-infrared wavelengths as nanorods are introduced into the pulsatile bloodstream of the subject and quantifies the circulating dose in near real-time in terms of optical density units (OD) [26], [27], [28]. An OD unit refers to the quantity of absorbance of the nanorods. The quantity of absorbance of the nanorods is indicative of the actual concentration of nanorods circulating at that time.

The experiment in which the data was collected employed two groups of ~20g BALB/c mice to examine the variability of nanorod circulation parameters and their effects on related clinical pharmacokinetic variables such as tumor uptake. The ~100 OD nanorods were intravenously injected at dosages of either 4.5μL/gm (1x) or 9μL/gm (2x) body weight at the rate of 18μl/min. At discrete time points post-injection, the NanoTracker was placed on the tail of the mouse and measurements were taken at regular intervals until which time the observed optical density reached a level of 1 OD $\pm$10%. The data was later used to produce a bioavailability curve and to compute typical measurements of performance such as AUC and half-life. The bioavailability curve that was produced here is not the same as that which is found by any of the least error models presented in this chapter.

2.2 Least Error Models

It is important to be aware that, as the measurements were taken at discrete time intervals and not continuously for the duration of the experiment, the highest or lowest points in the observed data do not necessary reflect the actually highest

and lowest points that occur in reality. For this reason, more points are interpolated using the observed data points. This process is described in Subsection 2.2.1. The data is separated into two phases: the injection phase, or uptake, and the elimination phase, or retention, which refers to how long the nanoparticles are actually staying in the body. Currently, the literature mostly focuses on modeling the retention phase by itself [17]. As it is important for this study to model both phases of the data, three different models are created and a minimal search algorithm is performed using MATLAB® in order to find the best fit between the experimental data and the mathematical models.

2.2.1 Error Determination

The function against which the respective models were compared was a piece-wise exponential function. This was created by determining an exponential function which fit each pair of consecutive experimental data points. The algorithm was written to insure the function started at zero for each set of data and also terminated at the final data point (as opposed to assuming an exponential decay or rise past that point). For the sake of conciseness, this function will be defined as $A(t)$.

Initially, the error was calculated using the standard Euclidian norm, shown in (2.1)

$$\sqrt{\left(\sum_{i=1}^{N}((y_i - \tilde{y_i})^2)\right)}, \tag{2.1}$$

where $N :=$ total number of points in $A(t)$, $y - \tilde{y} :=$ the error in the y-direction between the model to be found and the approximated experimental function $A(t)$. This calculation evolved to evaluating the error using the standard R-squared value

for ease of comparison to other models in the literature and also because this is the more generally accepted error calculation. The R-squared value is defined in (2.2)

$$R^2 = 1 - \frac{\sum_i((y_i - \tilde{y}_i)^2)}{\sum_i((y_i - \bar{y})^2)}, \tag{2.2}$$

where $y - \tilde{y} :=$ the error in the y-direction between the model to be found and the approximated experimental function $A(t)$ and $y_i - \bar{y} :=$ the difference between the function $A(t)$ and the mean value of $A(t)$. A model which yields an R-squared value close to one is considered a good fit and implies low errors.

Though utilizing the calculated R-squared as the value to be minimized when finding each model was appropriate for comparison purposes, it proved to be a weak determination of overall error between a model and $A(t)$ as it only took the error in y-direction into account. It was observed in the models that though there may have been a large difference in the y-direction, the values in the x-direction were quite close. In order to better represent the overall error for each model, the Total Least Squared (TLS) method given in [30] was performed. This method found the orthogonal distance between each point on the particular model and the nearest point (considering both the x and y-directions) in $A(t)$. The total error in this method was defined as the sum of these distances squared. As this value is comparable to the numerator of (2.2), in order to be able to compare each error calculation with ease, the 'TLS-squared' value is calculated by replacing the numerator of (2.2) with the TLS error value. Both the R-squared and 'TLS-squared' error values are calculated for each model that is presented and values close to one imply good fits.

2.2.2 Rational Model

Both the uptake and retention phases of the data were initially modeled using a rational expression. As this expression models both the uptake and the retention phase, it is particularly useful for predictive purposes such as early diagnosis of adverse reactions to the nanoparticles. After considering several different functions (polynomials of varying degrees, logistic equation, and trigonometric functions), the following equation was found to represent the experimental data well and yielded low error when the aforementioned minimal search algorithm was performed:

$$C_B(t) = \frac{\alpha * t}{\beta * t^2 + \gamma}, \tag{2.3}$$

with α, β, and γ being real-valued parameters determined from the minimal search algorithm and t time (in minutes). As an example, Figure 2.1 shows this model with its corresponding R-squared value for one particular mouse.

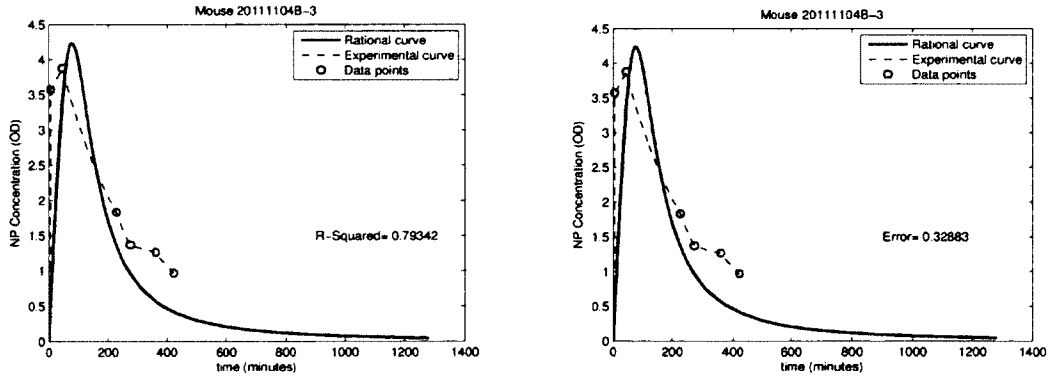

Figure 2.1: Approximated rational curve found using R-squared (left) and TLS (right)

This function yields acceptably low R-squared values and gives a good estimation of the uptake and retention phases of the nanoparticles. However, the peak absorbance value (in OD units) is skewed towards the right of the experimental peak for each mouse modeled, and it also tends to show too sharp of a drop immediately following the peak absorbance when compared to experimental observations.

2.2.3 Exponential Model

Though the rational model is useful for predictive purposes, an exponential decay which models only the elimination of nanoparticles from the bloodstream is the more generally accepted model in pharmacokinetics [17]. Of course, even though the nanoparticles are not drugs and are generally inert, they must still clear them, so the exponential model which highlights the elimination phase was naturally considered as a possibility. This model begins at the peak data point, where the nanoparticles are at the highest observed concentration in the bloodstream. Dr. O'Neal and his team theorize that the reason for the sharp drop in concentration after the nanoparticle peak in the algebraic model is because of poorly coated nanoparticles that are in the batch. As the nanoparticles must be coated with something to keep the body from eliminating them immediately upon detection, the nanoparticles that are not properly coated (and there are some in every batch), and therefore easily detected by the body's reticulo-endothelial system, will be eliminated very quickly. This model helps to lessen that drop off by not taking the improperly coated nanoparticles into account as much as (2.3). An exponential decay function is used:

$$C_B(t) = \alpha * e^{-\beta * t}, \tag{2.4}$$

where α and β are real-valued parameters and t is time (in minutes). These parameters were found in the same way as those for (2.3) while only using the experimental data from the retention phase. As with the rational model, this yielded low error when compared to the experimental data. Figure 2.2 shows the exponential plot for the same mouse as depicted in Figure 2.1. It is also of interest to find the area under

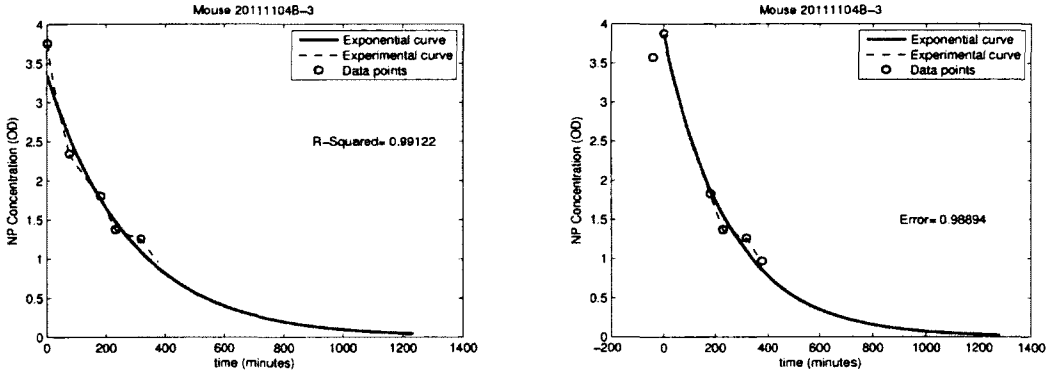

Figure 2.2: Approximated exponential curve found using R-squared (left) and TLS (right)

the curve (AUC) of each fit for each mouse as it can be telling of the total uptake of the nanoparticles in the body. With that in mind, while finding the best fit models, code was also run to find the maximum values for the rational fit, the area under the curve for both fits, and the half-life for the nanoparticle circulation in the bloodstream. Just as the uptake can be found using the area under the curve, the retention is seen by looking at the half-life [17]. The area under the curve was found using Simpson's

quadrature with the best fit array and the half-life by finding the time at which the absorbance is half that of the maximum value of the best-fit model.

2.2.4 Absolute Value Model

The rational model was useful in predictions but, though it yielded good R-squared values, was found to be skewed towards the elimination phase of the curve. That is, it took more time on average in the prediction models to reach the maximum absorbance than was actually being observed in experiments. In an attempt to solve this problem, a new model was used that showed a sharper rise to help account more properly for the accumulation phase of the curve. This function has been found to yield similar R-squared values overall but showed a more realistic shape when compared to the experimental data. Several exponential values were tested before arriving at the equation:

$$C_B(t) = -\left|\alpha * t^{\frac{2}{3}} - \beta\right| + \beta + \gamma * t^{\frac{3}{4}}, \tag{2.5}$$

with α, β, and γ being real-valued parameters and t is time (in minutes). The constants are found in the same way as those of (2.5) and (2.4). Figure 2.3 shows a plot of this fit for the same mouse displayed in Figures 2.1 and 2.2.

2.2.5 Piecewise Model

In order to obtain a model that would have a still better fit for both the uptake and retention phases, a concatenation of functions to create a piecewise function was done. As it is the goal of this project to be able to create these models in real time, it was necessary at this point to use functions that had already been found to yield a

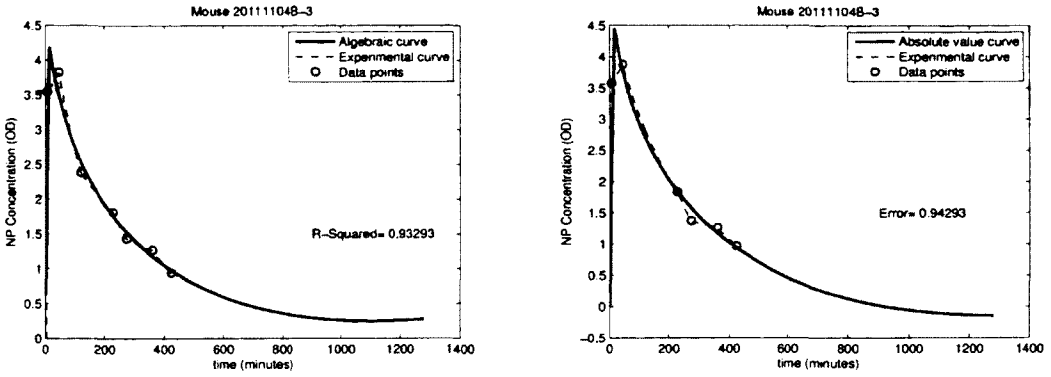

Figure 2.3: Approximated absolute value curve found using R-squared (left) and TLS (right)

good fit for either the uptake or retention phase. With that in mind, the exponential fit was used for the retention phase and different injection profiles were considered for the uptake.

Four injection profiles per dosage group are considered in this work. The first is linear, thus indicating a linear rate, the second is a positive quadratic, indicating an increase in the rate of injection as time progresses, the third is a negative quadratic, indicating a faster rate of injection initially that levels off toward the end of the injection time window, and the last is an exponential curve, indicating an exponential rate. The four injection profiles per dosage, denoted $I_i(t)$ with $i = 1, 2, 3, 4$, were designed to satisfy the same conditions as those specified for (2.4), thus yielding

$$\begin{aligned} I_1(t) &= (\tfrac{\alpha}{\eta})t + \alpha, \\ I_2(t) &= (\tfrac{\alpha}{\eta^2})(t+\eta)^2, \\ I_3(t) &= -(\tfrac{\alpha}{\eta^2})t^2 + \alpha, \\ I_4(t) &= e^{\frac{\ln(\alpha+1)}{\eta}(t+\eta)} - 1, \end{aligned} \tag{2.6}$$

with α from (2.4), t is time, and η equal to the injection time (10 minutes or 0.1667 hours unless otherwise specified). These profiles are shown for the average mouse in each data set (1x and 2x) in Figure 2.4 and are described further in Chapter 3. Each of these profiles are used to represent the injection phase of the experiment with

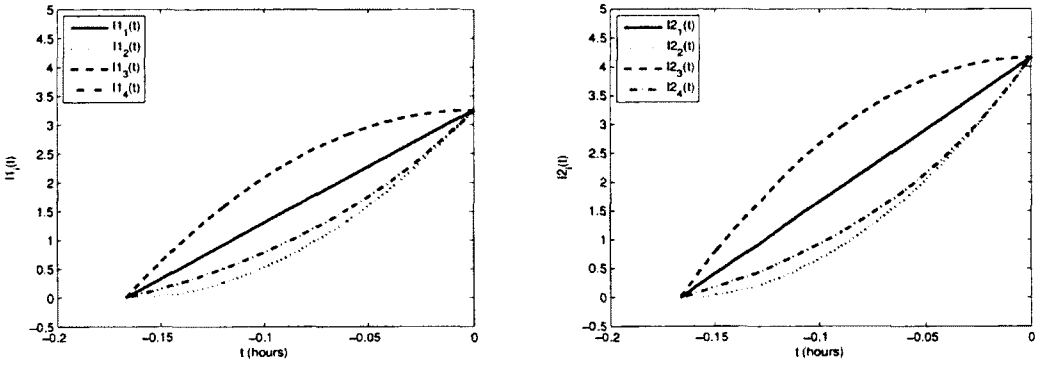

Figure 2.4: Injection Profiles for 1x Mouse (left) and 2x Mouse (right) (in OD)

the already found exponential function representing the retention phase. In order to have a more ideal control effort, the negative quadratic injection profile is used here yielding the equation

$$C_B(t) = \begin{cases} -(\frac{\alpha}{\eta^2})t^2 + \alpha & : 0 < t \leq t_i \\ \alpha * e^{-\beta*(t-t_i)} & : t > t_i \end{cases}, \tag{2.7}$$

where α and η are the same as in (2.6). This gives the model shown in Figure 2.5. As this model is actually a concatenation of functions and is not found using a minimal search algorithm, it is not necessary to compare the different error terms in this case. These error calculations have essentially already been found during the calculation of the exponential model. For that reason, this model is only shown with its respective R-squared value.

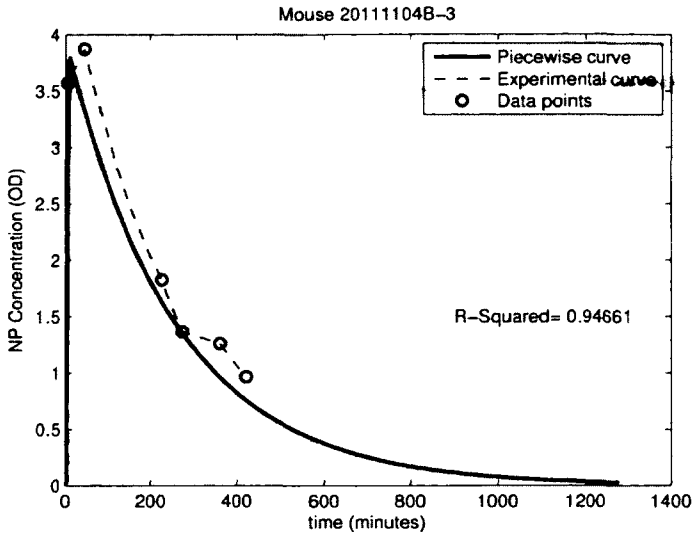

Figure 2.5: Approximated piecewise curve

2.3 Results

There were several different models presented and each gave a different insight into how the experimental data behaves in real time. The R-squared values for each model for each mouse were found using the residuals in the y-direction with the interpolation experimental data points vs. the points found in each best fit model, as described in Subsection 2.2.1. These values are shown in Table 2.1.

When analyzing the mean and median shown in Table 2.1 we can see that the values for each model set are quite close with the exception of the piecewise models where the mean= .759 and the median= .915. This discrepancy most likely implies outliers in the data set for that model which are assumed to be caused by the weakness in the R-squared value. It is important to note that, since only the vertical values are considered in the R-squared calculation, some of the values may be quite low even though the figures show that model appears accurate. The vertical values were

Table 2.1: R-Squared Values per Mouse

Mouse	Rational R^2	Abs. Value R^2	Exponential R^2	Piecewise R^2
20111104A-1	0.681	0.809	0.998	0.212
20120120C-3	0.499	0.861	0.867	0.947
20111202A-0	0.558	0.936	0.993	0.908
20120120C-5	0.559	0.862	0.972	0.771
20111104A-3	0.479	0.945	0.928	0.925
20111202A-1	0.438	0.933	0.972	0.892
20111202B-1	0.562	0.941	0.989	0.915
20111202A-2	0.734	0.704	0.919	0.276
20120120A-0	0.185	0.815	0.933	0.931
20111104B-1	0.819	0.672	0.984	0.132
20111104A-5	0.665	0.672	0.979	0.350
20111202B-3	0.802	0.652	0.992	0.639
20111104B-3	0.793	0.936	0.997	0.947
20111202B-2	0.711	0.853	0.991	0.987
20120120D-0	0.580	0.963	0.978	0.958
20120220A-3-5	0.563	0.920	0.983	0.979
20120220A-5	0.537	0.961	0.982	0.976
Mean R^2	0.596	0.850	0.969	0.759
Median R^2	0.563	0.862	0.982	0.915

considered as well in the TLS method (as discussed in Subsection 2.2.1) though using these considerations tended to produce very similar models as those found using the R-squared calculation. That being said, the mean and median values shown for the exponential models are considerably close to one, meaning that model is consistently accurate. It makes sense that this model shows the most accurate results as it only models the elimination phase when the injection phase appeared to be the main source of error for the other models. Due to the lower R-squared values for the models that show both the injection and elimination phases it can be assumed that the injection phase of the experiment is more difficult to predict than the elimination phase. This is most likely because of the lack of experimental data points for this phase of the

experiment. The sparse data collection during the injection forces the models to make more assumptions than are needed during the elimination phase where more data points were given. The absolute value model appears to be the most accurate model which takes both the injection and elimination phase into account. However, as discussed above, the piecewise model appears to describe the data accurately as well, with the exception of the few values in the data set already discussed.

CHAPTER 3

STATISTICAL EVALUATIONS

With the best fits found as described in Chapter 2 for each of the mice for each of the models, it is necessary to perform statistical evaluations to ensure first that the results make biological sense and also to make certain that averages of each data set can be taken. The Spearman Rank Correlation test, described in Section 3.1, was chosen to test how well certain values in the data compared to others which is descriptive of the raw data found in the experiment. The Wilcoxon Signed Rank test described in Section 3.2 showed whether all of the least fits for a particular model could be averaged to create a "master mouse" without loss of generality. The non-parametric tests were chosen due to the small data sets and lack of normality within the sets [31]. The freeware program R was used for this analysis.

3.1 Spearman Rank Correlation

The first test run was the Spearman rank correlation in order to investigate how well certain values within the data correlated. The results are shown in Table 3.1, with a ρ close to $\pm$ 1 implying a high correlation. The value ρ is a nonparametric measure of statistical dependance between any two variables. As can be seen in Table 3.1, almost none of the data comparisons yielded high correlation coefficients.

While these results are of interest to the biological portion of the experiment, they do not have a negative effect on this analysis.

Table 3.1: Spearman Rank Correlation Results

Data Sets Tested	ρ
*max absorbance for 1x rational model vs. AUC for 1x rational model	0.2771084
*max absorbance for 1x abs. value model vs. AUC for 1x abs. value model	0.3012048
max absorbance for 2x rational model vs. AUC for 2x rational model	0.6727273
max absorbance for 2x abs. value model vs. AUC for 2x abs. value model	0.60
*AUC for 1x exp. model vs. AUC for 1x abs. value model	0.5421687
*AUC for 1x exp. model vs. AUC for 1x rational model	0.5421687
AUC for 2x exp. model vs. AUC for 2x abs. value model	0.8545455
AUC for 2x exp. model vs. AUC for 2x rational model	0.8545455

The * in Table 3.1 implies that the exact p-value could not be computed with ties. As this warning came up when the test was run, it was appropriate to report it here. However, since the outcome of the test is dependent on ρ and not p, the fact that the p-value could not be computed on some of the tests is irrelevant. The first set of tests run evaluated the level of correlation between the maximum values calculated in the models and the AUC for the respective model. As the highest of these correlations found was 0.6727 it is clear that there exists no clear correlation between these values. This result is not what was expected as it would seem reasonable that the higher the maximum value of the model is, the higher the AUC would be as well. That assumption, however, is not supported by this analysis.

The second group of values (the bottom four in Table 3.1) test the correlation between the AUC for the exponential models and the AUC for rational or absolute value models. Though the values for the 1x models are quite low, the 2x models seem to have a high correlation. It is unusual that the different initial dosages would produce such different results in this test but it is expected that the exponential model would have a good correlation with the other two. This analysis is taken into account in Chapters 4 and 5 in the discussion of the different controllers that are presented.

3.2 Wilcoxon Signed Rank

The Wilcoxon Signed Rank Test was performed on each individual set of data, testing if the mean of the data is statistically equal to the median. The null hypothesis for the test on each data set was that the median is equal to the mean, which would imply that the data is closely related with the alternative hypothesis being that mean and median are not equal, or that the data is not closely related. The null hypothesis was rejected if the found p-value was less than α (which was chosen to be 0.05) and was accepted otherwise. The results of this test are quite significant as negative results would prevent the analysis from moving forward for that particular data set. The results from this test are shown in Table 3.2 with * implying the same warning as was in Table 3.1. It is shown that the data within each set are statistically similar as the p-value that was found was higher than the chosen α. Though the exact p-value could not be determined for certain sets, the close calculation which was found was determined to be a good estimate. As the sets were all found to be statistically similar we are now able to average each set without concern of misrepresenting the data.

Table 3.2: Wilcoxon Signed Rank Test Results

Data Set Tested	p-value
max absorbance for 2x rational models	0.7695
max absorbance for 2x abs. value models	1.0
AUC for 2x rational models	0.9219
AUC for 2x exponential models	0.9219
AUC for 2x abs. value models	0.9219
max absorbance for 1x rational models	*0.9441
max absorbance for 1x abs. value models	*0.9441
AUC for 1x rational models	*0.9441
AUC for 1x exponential models	*1.0
AUC for 1x abs. value models	*0.9441

3.3 Confidence and Prediction Intervals

As all of the mice within each individual data set were found to be statistically similar, an average of each data set could be performed to create a "master mouse" of all of the models. With these "master mice", confidence and prediction intervals were calculated using MATLAB®.

The difference between confidence and prediction intervals is an important distinction to make. As an example, an 80% confidence interval implies that if 100 similar samples were drawn, in 80 out of 100 tests, the mean absorbance measure would fall in that interval. The confidence interval is a good indication of how well the mean of the data has been determined. A prediction interval gives a range of where the next data point sampled can be expected. That is, for example, for an 85% prediction interval, there is an 85% probability that the next sampled data point will fall within that range. This interval tells about the distribution of the data, rather than the uncertainty in determining the mean [2], [24].

The confidence intervals were calculated at 80% and 90% for each data set. To find these intervals within each set, the absorption values at each time point were first averaged in order to create the master mouse for that data set. The standard deviation was then found using the built in MATLAB® function. For the 1x data sets, the 80% intervals were calculated at each time point by taking the average absorbance ± 1.383×standard deviation and the 90% bounds by average absorbance ± 1.833×standard deviation. And for the 2x data sets: 80% bounds by average absorbance ± 1.415*standard deviation, 90% by average absorbance ± 1.895*standard deviation. Each of these values were found in the standard t-distribution table according to the number of mice in each data set.

The prediction intervals for each data set were calculated at 85% for each time value so that a mostly smooth function was created for the upper and lower bounds of the intervals. In order to calculate the intervals, the absorbance values for each time set first had to be arranged in increasing order. Once the data was in increasing order, the central 85% of the data was taken to be the prediction set for that time point.

For ease of comparison, the exponential models with their confidence and prediction intervals are shown in Figure 3.1. Figure 3.2 shows the 1x and 2x rational models with their respective confidence and prediction intervals, found in the same manner as the exponential intervals. Similarly found were the absolute value models for the 1x and 2x data sets, shown in Figure 3.3 and the piecewise models shown in Figure 3.4. The intervals for these figures are shown with 90% confidence intervals being the outer dashed lines and the 80% confidence intervals being the inner dotted

line. The 85% prediction intervals are represented by the two solid lines surrounding the center line (with the center line being the model itself).

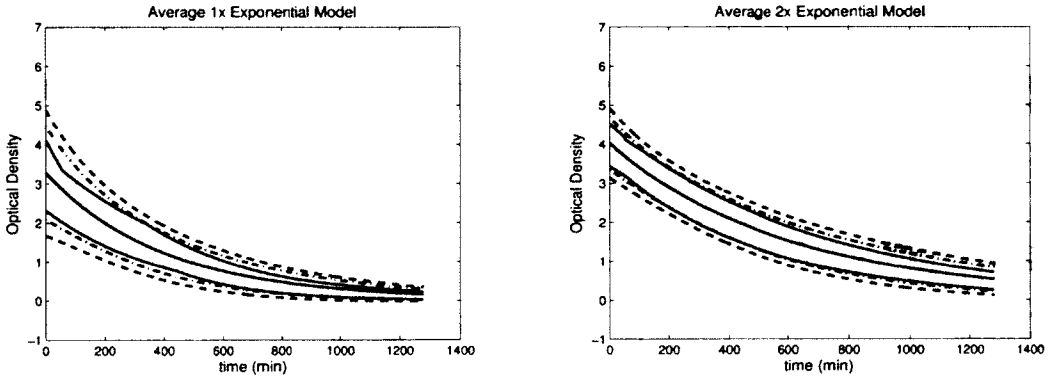

Figure 3.1: Exponential 1x Model (left), Exponential 2x Model (right)

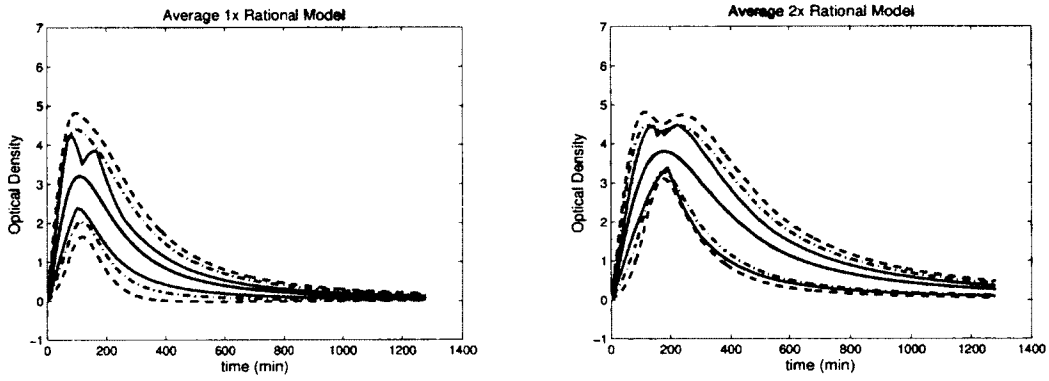

Figure 3.2: Rational 1x Model (left), Rational 2x Model (right)

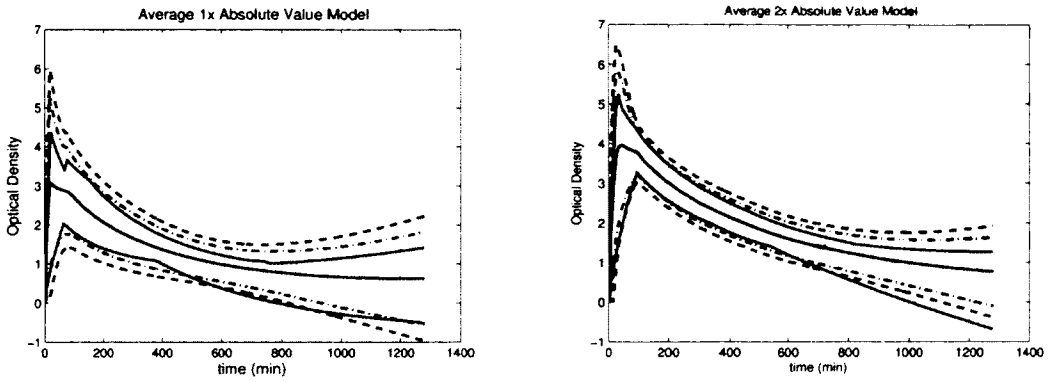

Figure 3.3: Abs. Value 1x Model (left), Abs. Value 2x Model (right)

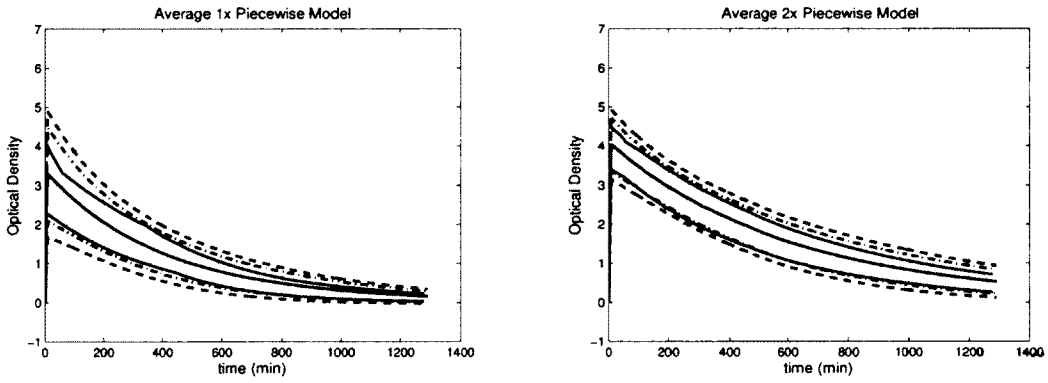

Figure 3.4: Piecewise 1x Model (left), Piecewise 2x Model (right)

The prediction intervals are different from the confidence intervals as they give a range of where the next experimental data point should fall as opposed to where the mean of future data sets would fall. The fact that the different intervals are close in value is a good indication the experimental data sets are closely related. Each of these intervals can be useful for the identification of untoward reactions when applied in an experimental setting by comparing data points measured in real time with the 'Master Mouse' for the respective dosage and its confidence and prediction intervals.

Data points falling outside of these intervals would be a flag for further investigation to determine untoward reactions and/or to change to dosage scheme accordingly.

CHAPTER 4

LQR TRACKING CONTROL

As the least error mathematical models have been found in Chapter 2 and confirmed through the statistical evaluations in Chapter 3, we will now show how the exponential model is utilized in a state space feedback control framework to regulate the nanoparticles in the bloodstream. An equal time delay is also introduced in both the state and control input for the purpose of studying the alternate dosing strategies shown in (2.6). While only the exponential model is being controlled, the inclusion of the dosing strategies to account for the time delay creates a piecewise function which is identical to the piecewise function described in Chapter 2.

Clearly, (2.4) is the solution to the simple first order, linear ordinary differential equation

$$\dot{C}_B(t) = -\beta C_B(t), \tag{4.1}$$

where $\dot{C}_B(t) = \dfrac{dC_B(t)}{dt}$, $C_B(t = 0) = \gamma \in \mathbb{R}$ in (2.4), $-\beta \in \mathbb{R}$ is the exponential decay rate, and time $t = 0$ corresponds to the time when the nanoparticles are at their highest concentration in the bloodstream, which occurs at some delayed time after the nanoparticle injection. The two specific quantities of interest for comparison between the experimental data and the model are the nanoparticle half-life and the AUC, referring to area under the bloodstream nanoparticle concentration curve. The

half-life can be used to quantify nanoparticle retention, or how long the nanoparticles remain in the body. The area under the curve is important because it describes the total uptake of nanoparticles by the body. Table 4.1 shows a comparison between the experimental data and the model for these two quantities of interest with an * implying irrelevant results due to unrefined data, meaning that the set of experimental data points did not provide enough information to appropriately calculate the AUC. With

Table 4.1: Comparison Between Model and Experimental Results

Mouse ID	Model R^2	Model AUC (OD*min)	Exper. AUC (OD*min)	Model 1/2-life (min)	Exper. 1/2-life (min)
20111104A-1	1.00	2163	1981	507	488
20120120C-3	0.87	2725	2446	505	444
20111202A-0	0.99	1978	1747	465	499
20120120C-5	0.97	2916	2628	562	533
20111104A-3	0.93	1982	1828	305	347
20111202A-1	0.97	1931	1716	409	444
20111202B-1	0.99	2088	1851	349	350
20111202A-2	0.92	1769	1480	349	248
20120120A-0	0.93	2553	2300	496	444
20111104B-1	0.98	1100	743	339	365
20111104A-5	0.98	1880	1609	356	367
20111202B-3	0.99	964	701	234	247
20111104B-3	1.00	961	773	177	205
20111202B-2	1.00	915	*	283	272
20120120D-0	0.98	1815	1610	276	309
20120220A-3-5	0.98	1521	1212	326	330
20120220A-5	0.98	1206	1024	282	304
mean	0.97	1792	1603	366	370
median	0.98	1978	1788	349	350

the mean and median for each data set shown in Table 4.1 being close together we can assume that the data within each set do not have any extraneous values throwing off the set as a whole. The controller presented later in this chapter and also those presented in Chapter 5 aim to maximize the AUC and also lengthen the half life of

the mouse (increasing the AUC and lengthening the half-life would theoretically go hand in hand). After the half-life and area under the curve results were found for each mouse, statistical tests for similarity and correlations were run as described in Chapter 3.

Because it is of interest to investigate different injection rates, the rate effects on nanoparticle bioavailability, and maintaining the bloodstream nanoparticle concentration within an established therapeutic window, (4.1) is posed as a controlled, delay differential equation (DDE). Specifically of interest is the optimal control of the system with equal delays in both the state and control input. The general theory for the LQR control problem related to delay systems can be found in [6], [8], [13], [35], [36]. The model and control frameworks presented here will follow the more recent formulation presented in [7]. The system of interest is given by

$$\dot{C}_B(t) = -\beta C_B(t-h) + bu(t-h), \tag{4.2}$$

subject to the history function $C_B(s) = \phi(s) \in C([-h, 0]; \mathbb{R}^1)$ for all $s \in [-h, 0]$, where h is the time delay in hours, $C_B(t) \in \mathbb{R}^1$ is the system state representing concentration of nanoparticles in the bloodstream, $u(t) \in \mathbb{R}^1$ is the control input, b is a real-valued constant control input multiplier, and $-\beta \in \mathbb{R}$ is the exponential decay rate. With the inclusion of a delay in the state, (4.2) is an infinite-dimensional system (see, for example, [25]). This means that the function space has a basis set which is infinite which further means that the function cannot be represented using a finite set of simpler functions. From a practical standpoint, note that the time delay, h, will correspond to the length of time over which the nanoparticle injection is given,

and different history functions $\phi(s)$ (the same as those functions given in (2.6)) will correspond to the different injection profiles being considered.

4.1 Control Strategies

With (4.2) being a linear system, standard linear quadratic control techniques will be employed. The solution to this control problem, with equal time delays found in both the state and input, is found in [7] and summarized here, with appropriate modifications made to include tracking, similar to the derivation in [16]. The specific control objective of interest includes output tracking, for the purpose of regulating the bloodstream nanoparticle concentration to lie within a specified therapeutic window. This will be analyzed for multiple injection profiles, i.e. rates.

In considering a general linear system with time delay

$$\dot{x}(t) = A(t)x(t-h) + B(t)u(t-h), \tag{4.3}$$

with the usual assumptions as described in [7], the control implementation involves a Linear Quadratic Regulator (LQR) state tracking design, where the quadratic cost function to be minimized is

$$\begin{aligned} J &= \frac{1}{2}[x(T)]^T \psi[x(T)] + \frac{1}{2}\int_0^T u^T(s)R(s)u(s)\,ds \\ &\quad + \frac{1}{2}\int_0^T x^T(s)L(s)x(s)\,ds, \end{aligned} \tag{4.4}$$

and the tracking problem reduces to a disturbance-rejection problem of the form

$$\dot{x}(t) = A(t)x_1(t) + B(t)u_1(t) + w(t), \tag{4.5}$$

where $x_1(t) = x(t-h) = \xi(t-h) - \tilde{\xi}(t-h)$, $u_1(t) = u(t-h)$, $w(t)$ is represented by

$$w(t) = A(t)\tilde{\xi} - \dot{\tilde{\xi}} \neq 0, \tag{4.6}$$

ξ is the state of some original dynamical linear system of interest,

$$\dot{\xi}(t) = A_0(t)\xi(t-h) + B_0(t)u(t-h) + z, \tag{4.7}$$

$\tilde{\xi}$ is the known desired state target of (4.7), and z is zero-mean, Gaussian, white noise.

The Hamiltonian for the optimal control problem (4.4), (4.5) is defined as

$$\begin{aligned} H(x,u,q,t) &= \frac{1}{2}u^T R(t)u + \frac{1}{2}x^T L(t)x \\ &\quad + q^T[A(t)x_1 + B(t)u_1 + w]. \end{aligned} \tag{4.8}$$

For the purpose of minimizing the Hamiltonian with respect to u, the gradient of (4.8) is set equal to zero. Then solving for u yields the optimal control

$$u^* = -R^{-1}(t)M^T(t)B^T(t)q(t), \tag{4.9}$$

where $M(t) := \dfrac{\partial u_1(t)}{\partial u}$. Selecting a general quadratic form

$$J^*(x,t) = \frac{1}{2}x^T(t)Q(t)x(t) + b^T(t)x(t) + c(t) \tag{4.10}$$

for the solution to the Hamilton-Jacobi optimization equation, to account for the disturbance term $w(t)$, yields the co-state

$$q(t) = -\frac{\partial J^*(x,t)}{\partial x} = -Q(t)x(t) - b(t). \tag{4.11}$$

Then, with arguments of variables omitted from this point forward in the derivation for conciseness, the Hamilton-Jacobi optimization equation becomes

$$\begin{aligned} -\frac{1}{2}x^T\dot{Q}x - \dot{b}^T x - \dot{c} = \min_u \Big\{ &\frac{1}{2}x^T L x + \frac{1}{2}u^T R u \\ &+(-Qx-b)^T(Ax_1 + Bu_1 + A\tilde{\xi})\Big\}, \end{aligned} \tag{4.12}$$

thereby yielding the optimal control

$$u^* = R^{-1}M^T B^T(Qx+b). \tag{4.13}$$

Therefore, values for Q, M, and b must be determined. To determine Q, consider the co-state equation $\frac{dq(t)}{dt} = -\frac{\partial H}{\partial x}$, which yields

$$Q\dot{x} + \dot{Q}x + \dot{b} = Lx + A^T M_1 q, \tag{4.14}$$

where $M_1 := \frac{\partial x_1}{\partial x}$. Now substituting (4.11), (4.5), and then (4.13) into (4.14) yields

$$\begin{aligned} \dot{Q}x + QAx(t-h) + QB(R^{-1}M^T B^T Qx + R^{-1}M^T B^T b) \\ +Qw + \dot{b} = Lx - A^T M_1 Qx - A^T M_1 b. \end{aligned} \tag{4.15}$$

Differentiating (4.15) with respect to x and simplifying because M is the identity matrix per the argument in [7] produces the quasi-Riccati equation

$$\dot{Q} = -QM_1A - QBR^{-1}B^TQ + L - A^TM_1Q, \tag{4.16}$$

where $M_1 = 0$ for $t \in [0, h)$ and $M_1 = I$ for $t \geq h$, per [7]. Note that while the co-state selected in this work differs from that in [7], to accommodate for a control tracking objective here, the arguments to determine the values of M and M_1 are identical. To determine b, the optimal control (4.13) is substituted into the Hamilton-Jacobi equation optimization (4.12) and different powers of x are equated to obtain

$$\dot{b} = [A + BR^{-1}B^TQ]^T b + Qw. \tag{4.17}$$

Note that the solution for c in (4.10) is irrelevant for the control design sought here, and thus, the differential equation is not shown. Because of the boundary conditions $J^*(x,T) = \frac{1}{2}[x(T)]^T\psi[x(T)]$ for all x, there also exist the boundary conditions $Q(T) = -\psi$ and $b(T) = 0$. After the computation of Q and b, the optimal control law is written as

$$u^* = R^{-1}B^TQ(\xi - \tilde{\xi}) + R^{-1}B^Tb, \tag{4.18}$$

which is then implemented in (4.5).

4.2 Numerical Results

The numerical results presented here correspond to each of the 'Master Mice' presented in Chapter 3. This is because it is desired to consider the predictability of nanoparticle bioavailability for individual 'patients' and, therefore, predicting for the average mice is the most appropriate way to test the method. The parameters of best fit for (4.1) were determined to be

$$\gamma = (3.2475, 4.1573), \beta = (0.135, 0.095), \tag{4.19}$$

for the respective 1x and 2x models following an injection that began ten minutes earlier with the injection profiles described in (2.6). Because gold nanoparticles are devices, as opposed to medications, and only activated through laser, there is no maximum nanoparticle level for a patient. However, because it is desired to expand this analysis to many drugs and treatments, it is important to minimize the excess dosages of the nanoparticles. It also efficient from an industrial point of view to

limit the total dose as nanoparticles do cost money to create. Also, the system is not controlled on the time interval $(0, 0.1667)$ hours, so the area under the control curve is only computed on $[0.1667, 20]$ hours. It was decided to end the model at 20 hours as the absorbance value has dropped below functional levels by that time. The controller plots for each of the injection profiles can be found in Figures 4.1 and 4.2 for the 1x and 2x 'Master Mice', respectively. The plots show no distinguishable visual difference between the controllers required by each of the injection profiles.

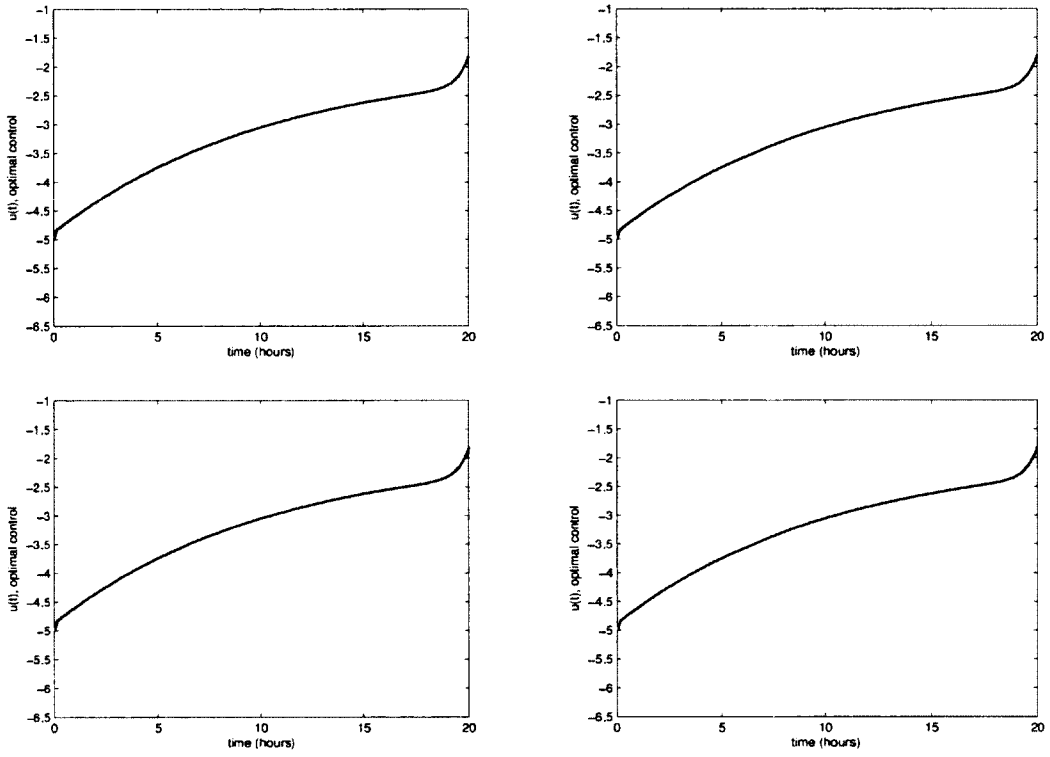

Figure 4.1: Controllers $u(t)$: Corresponding to: $I1_1(t)$ (upper left), $I1_2(t)$ (upper right), $I1_3(t)$ (lower left), $I1_4(t)$ (lower right),

To calculate the control effort required to achieve each of the injection profiles and steer the bloodstream nanoparticle concentration to .5*maximum absorbance over the course of a 20 hour time interval, the area under the absolute value of the control

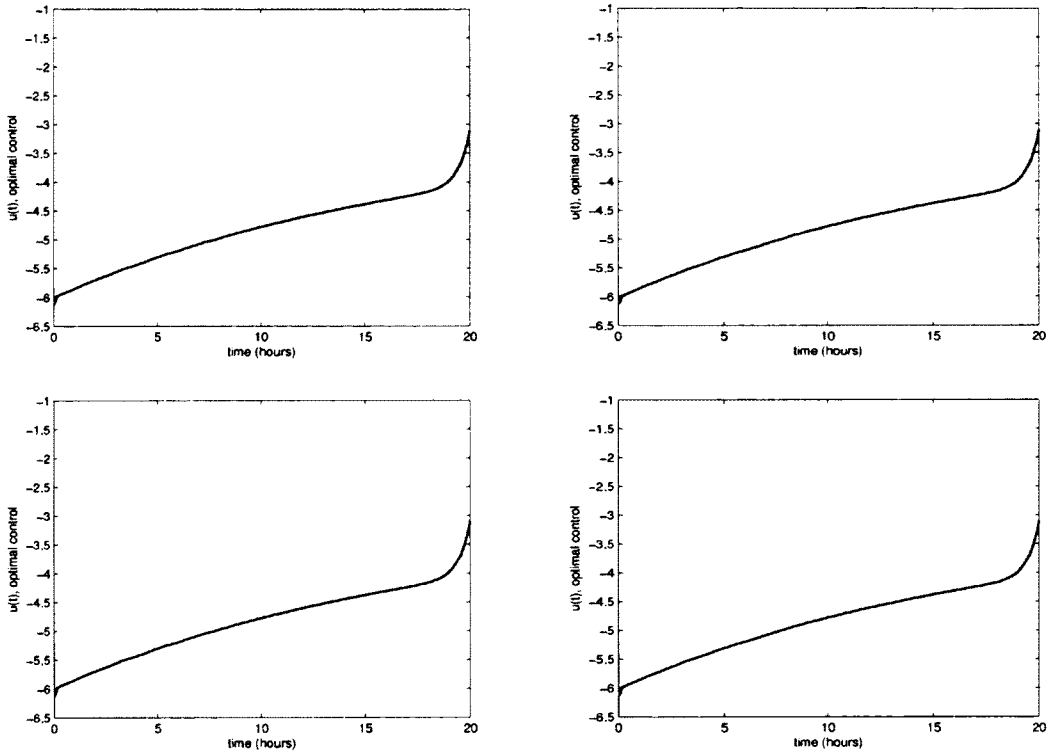

Figure 4.2: Controllers $u(t)$: Corresponding to: $I2_1(t)$ (upper left), $I2_2(t)$ (upper right), $I2_3(t)$ (lower left), $I2_4(t)$ (lower right),

curve $u(t)$ is added to the area under the corresponding injection profile curve. These results are found in Table 4.2. The required control effort is quite similar for each of the injection profiles, with the positive quadratic rate requiring the least amount of nanoparticles for each dosage group. Note that for all t, the control effort required for the various profiles follows the order $I_2 < I_4 < I_1 < I_3$ for each dosage group. However, for $t \in [-0.1667, 0]$, the control effort required for I_3 is the largest of all the injections for each dosage group while for $t \in [0.1667, 20]$, the control effort for I_3 is the smallest of all the injection profiles. It appears that the negative quadratic rate of injection found through using the I_3 profile allows the bloodstream nanoparticle concentration to "build up" so that fewer nanoparticles are needed later to achieve

the desired target, thus providing for a more efficient use of resources. I_1 follows a similar pattern for each dosage group and therefore also appears to provide for a more efficient injection. Given these results, it was determined that using the negative

Table 4.2: Control Efforts for Corresponding Injection Profiles (OD)

Injection	$t \in [-0.1667, 0]$	$t \in [0.1667, 20]$	Total Effort
$I1_1(t)$	0.2707	64.3755	64.6462
$I1_2(t)$	0.1805	64.4558	64.6363
$I1_3(t)$	0.3609	64.2951	64.6560
$I1_4(t)$	0.2076	64.4321	64.6397
$I2_1(t)$	0.3465	97.2718	97.6183
$I2_2(t)$	0.2310	97.3561	97.5871
$I2_3(t)$	0.4620	97.1875	97.6495
$I2_4(t)$	0.2558	97.3386	97.5944

quadratic injection profile is the most efficient. Using this injection, (4.2) was plotted and shown in Figures 4.3 and 4.4 with their respective uncontrolled models for ease of comparison.

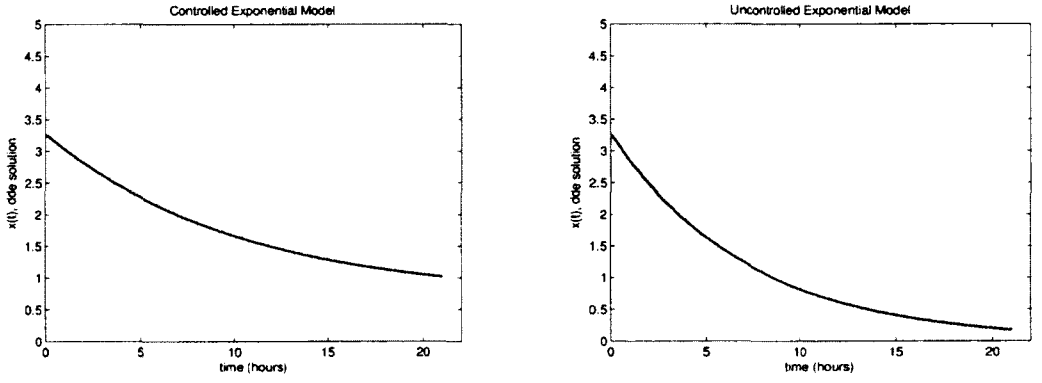

Figure 4.3: Controlled 1x Model (left), Uncontrolled 1x Model (right)

4.3 Dosage Conversion

These models control the absorbance level (in OD) of the nanoparticles over time but it is necessary to convert the values from the measurement to μL else, as

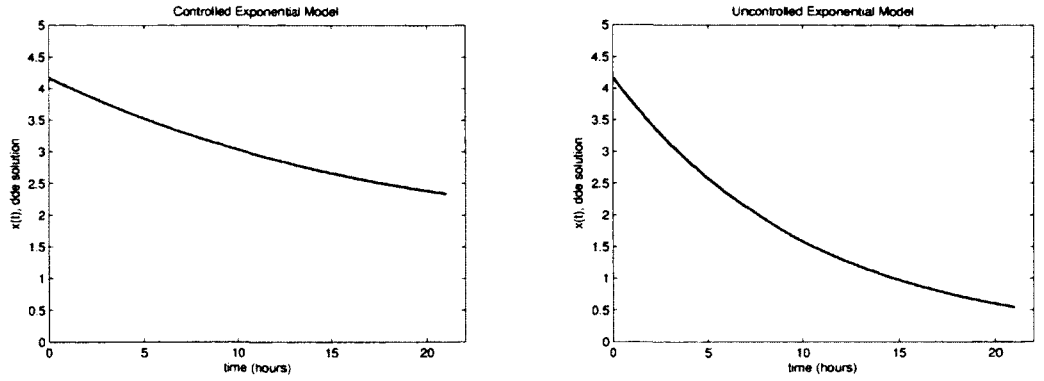

Figure 4.4: Controlled 2x Model (left), Uncontrolled 2x Model (right)

injections are measured in μL and not OD, the results are not useful in a real time experiment. In order to accomplish this, the peak absorbance values from the 1x and 2x 'Master Mice' along with the μL injected were plotted and different functions were fitted to the plot. The exponential function (4.20) was found to be the most reasonable:

$$f(x) = 0.6533x^{0.3564}, \tag{4.20}$$

where $f(x)$ =absorbance in OD and x =amount injected in μL. Inversely (4.21)

$$f(y) = 3.3019y^{2.8058}, \tag{4.21}$$

gives the opposite conversion where $f(y)$ =amount injected in μL and y =aborbance value in OD. These equations yield values consistent with what is expected experimentally as the absorbance value rises quickly with the initial injection and then begins to level off over time. A sample table of points is given in Table 4.3 and the plot of (4.21) is given in Figure 4.5.

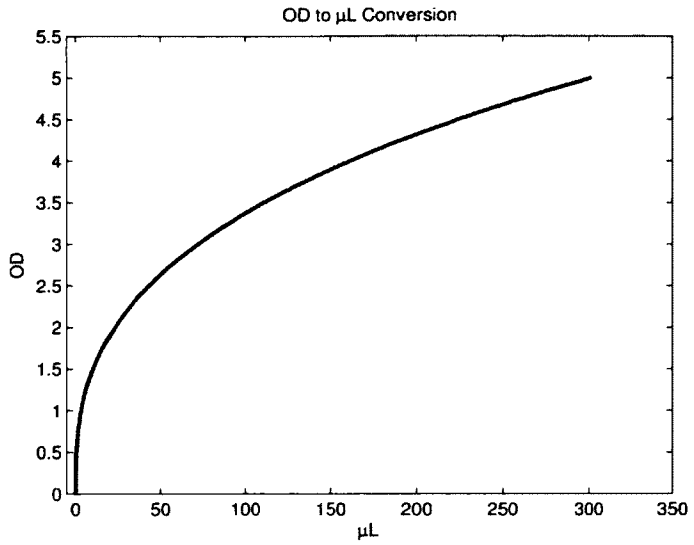

Figure 4.5: OD to μL Conversion

Table 4.3: Sample Values using the OD to μL Conversions

μL injected		Resultant absorbance (OD)
0		0.6533
90	(1x dose)	3.2475
180	(2x dose)	4.1575
360	(4x dose)	5.3233
720	(8x dose)	6.8150

Using (4.21), the total amount of μL needed to maintain the controller in the model given in (4.2) was calculated and those values are given in Table 4.4 along with the amounts used in experiments for the purpose of comparison. These values were determined by first converting the absorbance values from OD to μL for both the controlled and uncontrolled models, then summing the difference between the controlled and uncontrolled models of the converted values. The injection was found this way because, as the uncontrolled model gives the absorbance values when no injection (outside of the initial bolus injection) is made, the converted values from the uncontrolled model need to be subtracted from the calculation to ensure that

only the actual injection amount necessary in the controlled model is found. We are basically finding the area between the μL curves for the controlled and uncontrolled models.

Table 4.4: μL of Nanoparticles Required per Model

initial absorbance (OD)	target absorbance (OD)	uncontrolled model total dose (μL)	controlled model total dose (μL)
3.2475	1.6238	90	234.64
4.1573	2.0789	180	1080.92

The values in Table 4.4 reveal that using this method with the same initial injection as is used in the uncontrolled model we see that the controller requires quite a bit more μL to be injected than is ideal. However, as the absorbance level was kept at an ideal point with this method, it is worth investigating further to attempt to lower the overall control effort and, therefore, lower the necessary injection amount.

CHAPTER 5

CONTROLLER ANALYSIS

Because, in an experimental setting, each patient will have different reactions to a treatment and will need to be treated accordingly, it is important to investigate several different control strategies. This will provide more tools that can be called upon when this analysis is applied in real-time in an experimental setting. Using different strategies also helps to analyze the efficacy of any specific controller.

5.1 Further Investigation in the LQR Controller

Since the controller presented in Chapter 4 tracked efficiently, it was also of interest to consider a lower initial injection so that the total injection over time could be kept to minimum. Though it is unlikely that the amount of gold nanoparticles could ever build to a lethal level, it is important to look ahead to other treatments that may be able to be used with this analysis. Minimizing the injected amount needed will also help to reduce cost of treatment regardless of the treatment being used. With this in mind, each model was also run with an initial injection set to half of the original maximum absorbance of the respective models. That is, as the goal of the controller is to track to half the maximum absorbance, these models are now trying to track to the initial injection value. These plots are shown Figures 5.1 and 5.2 with their respective uncontrolled models. These models show that the applied

controller is able to to maintain the absorbance level of the nanoparticles at a level which is more acceptable than the uncontrolled models. As the LQR controller is designed to run in an optimal time frame, it is encouraging that the controller has an effect on the exponential decay model. The dosages required for these control efforts

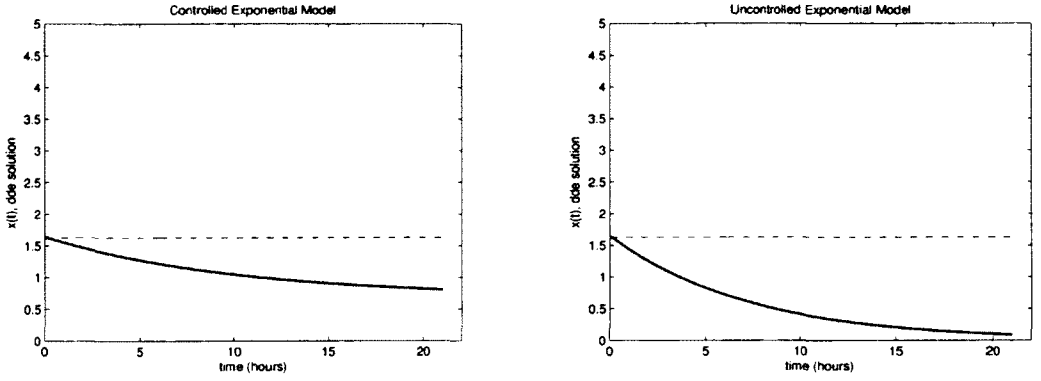

Figure 5.1: Controlled 1x Model (left), Uncontrolled 1x Model (right)

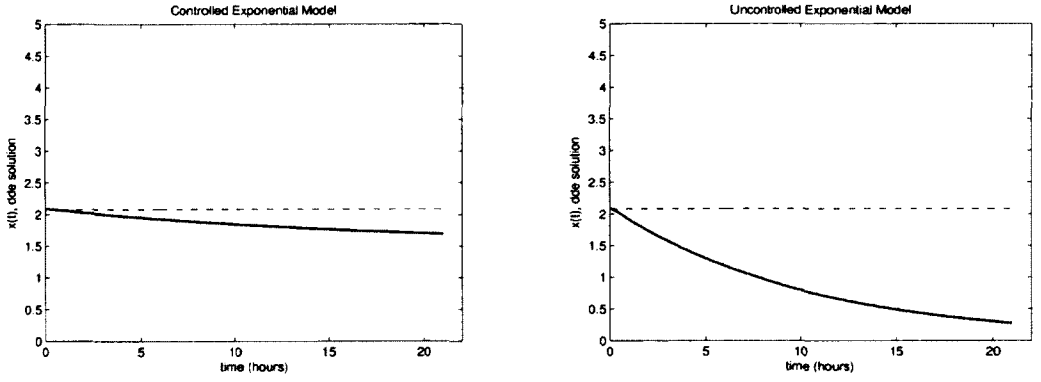

Figure 5.2: Controlled 2x Model (left), Uncontrolled 2x Model (right)

are presented in Table 5.1 along with those from the controller shown in Chapter 4 for ease of comparison. The dosages are found using the same process as that for the controller described in Chapter 4. The injections over time are shown in Figure 5.3. The values presented in Table 5.1 show that using a lower initial dose gives a

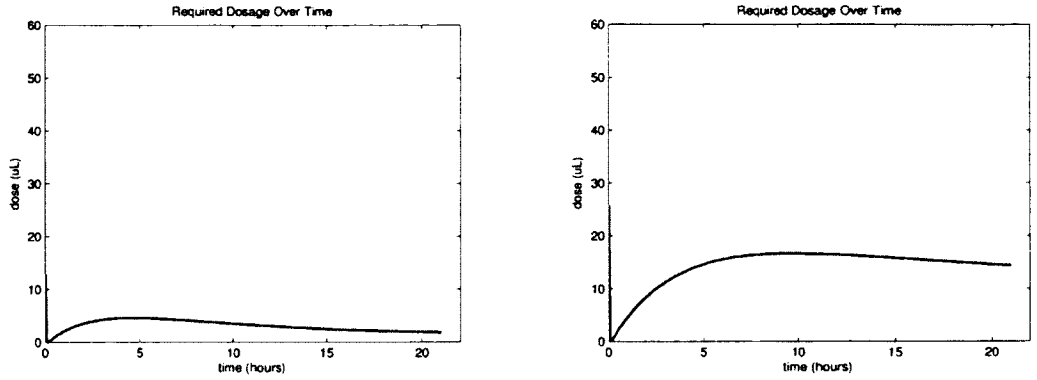

Figure 5.3: Controlled 1x Model (left) and 2x Model (right), in μL

Table 5.1: Total Dose of Each Control Strategy

	1x	2x	half 1x	half 2x
initial absorbance (OD)	3.2475	4.1573	1.6238	2.0789
target absorbance (OD)	1.6238	2.0789	1.6238	2.0789
LQR control total dose (μL)	234.64	1080.92	65.25	299.1

significantly more efficient method of control in terms of total injection. For the 2x model, the percent error between the controlled model and the tracking target is only 18.53%. However, for the 1x model, the calculated percent error is 50.15%. The low percent error for the 2x model is promising but the high error for the 1x model shows that this method may not be reliable when many different dosage groups are being considered. A model which requires a slightly higher overall injection but consistently keeps the absorbance closer to the tracking target may be preferred. Of course, too high of an overall injection is not ideal either.

5.2 Analysis of 'Control' Using Dirac Delta Functions

Though the controller discussed in Section 4.1 is interesting mathematically, it can not be easily replicated in a real time experiment with mice (which is important to realize as animal testing must be performed to confirm results before human testing can take place), mainly because the controller is a continuous feedback controller rather than a discrete controller. A discrete controller may also be useful in human testing as it may be simpler to detect untoward reactions with this type of control strategy than it would be with a continuous time control. With the injection not happening continuously, any untoward reaction would also be minimized when using this strategy. For these reasons, a good next step was to control the exponential function described in (4.1) using several Dirac delta functions to mathematically replicate bolus injections given at different time intervals. This equation is similar to (4.1) and is given by

$$\begin{aligned} \dot{C}_B(t) = -\beta C_B(t) + m_1\delta(t-h) + m_2\delta(t-2h) + m_3\delta(t-3h) \\ +m_4\delta(t-4h) + m_5\delta(t-5h) + m_6\delta(t-6h), \end{aligned} \tag{5.1}$$

where $\dot{C}_B(t) = \dfrac{dC_B(t)}{dt}$, $C_B(t=0) = \gamma \in \mathbb{R}$ in (4.1), $-\beta \in \mathbb{R}$ is the exponential decay rate, h is the time delay for the injections in hours, and m_i corresponds to the magnitude of the corresponding injection (represented by the Dirac delta functions) and is measured initially in OD and then converted to μL. m_1, m_2, m_3, m_4, m_5, m_6, and h were found by minimizing the TLS error that is calculated by comparing the solution to (5.1) against a constant function which was set equal to half the maximum value (which is considered to be in the therapeutic window for the nanoparticles),

following the examples in [21]. Finding these parameters proved to be more difficult than using the search algorithm described for the models in Chapter 2. First, (5.1) was solved analytically with a differential solver in MATLAB® and then evaluated using different values for each unknown parameter until a minimum error was found. The resulting plots over time are shown in Figures 5.4 and 5.5 for the 1x and 2x models, respectively. These plots show that several discrete injections are capable (for both the 1x and 2x models) of maintaining the absorbance value (in OD) at a level which would be considered within the therapeutic window of treatment for much of the experimental time frame.

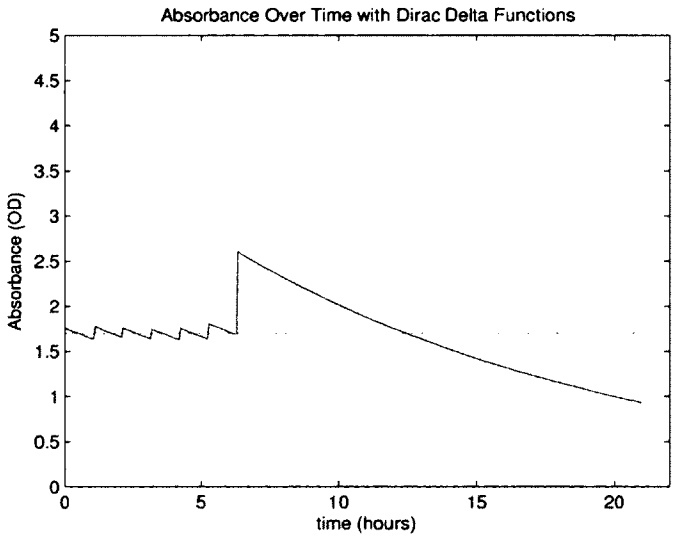

Figure 5.4: 1x Exponential Decay with Dirac Delta Functions

Table 5.2 shows the time between each injection given and the amount per injection. It was decided to limit the number of injections to six plus the initial injection. This was done for the purpose of feasibility in a real world setting. Of course, infinitely many injections would provide practically no error but that is not

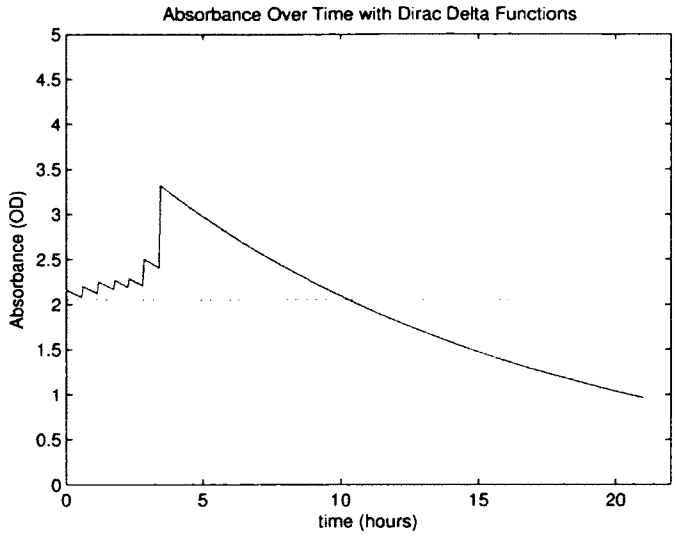

Figure 5.5: 2x Exponential Decay with Dirac Delta Functions

currently experimentally replicable. The time between injections was also restricted to be a constant value instead of varied. Tests were run with variable times between injections but these (much like having more injections) showed to take longer to run than would be reasonable in a real world setting. Having variable time steps, despite the longer time, did not provide significantly more effective 'control' of the exponential decay when compared to the constant time step. In the case of Dirac delta functions, the total injection amount is a simple sum of the each individual injection as this is not a continuous time controller. It is obvious from the values found in this analysis that having multiple smaller injections should provide a more efficient method of keeping the nanoparticle concentration within the assumed therapeutic window and would theoretically require a smaller injection amount overall than the original method of only one injection. When comparing the values from Tables 4.4 and 5.2 it seems clear

Table 5.2: Results Using Dirac Delta Functions

Time between injections	1.053hrs	0.567hrs
Initial Injection	16.172μL	28.722μL
2nd Injection (m_1)	3.395μL	4.480μL
3rd Injection (m_2)	2.561μL	4.840μL
4th Injection (m_3)	2.581μL	4.120μL
5th Injection (m_4)	3.015μL	3.869μL
6th Injection (m_5)	4.184μL	12.833μL
7th Injection (m_6)	34.161μL	56.939μL
Total Injection Amount	66.069μL	115.802μL
Experimental Injection	45.0μL	90.0μL

that the use of the Dirac delta functions as opposed to one continuous time controller is a more efficient choice in terms total amount of μL of nanoparticles needed.

5.3 PID Tracking Control of the Exponential Decay

The controller presented in Chapter 4 was determined to be appropriate for the given model. However, it was also of interest to investigate the use of a PID tracking control as it is a common control strategy used in the engineering and industrial settings [19]. With a PID tracking control like the one presented in [33] we can evaluate the possibility of tracking the model to a specific absorbtion value and also limiting the area under the curve so that the total injection is kept to a minimum. The model to be controlled is the same as that in Chapter 4 and given by (4.1).

5.3.1 Setup of the PID Controller

For this controller, the delay is only included in the control function and the model (in the time domain) is then generally presented as

$$\dot{x}(t) = A(t)x(t) + B(t)u(t-d), \tag{5.2}$$

where d represents the time delay. Unlike the LQR controller presented in 4.1, the PID controller utilizes three different gains, k_p, k_i, and k_d which represent the proportional gain, integral gain, and derivative gain, respectively. The control function u in the time domain is given by

$$u(t) = k_p e(t) + k_i \int e(t)\,dt + k_d \frac{de(t)}{dt}, \tag{5.3}$$

where k_p, k_i, and k_d are the gains to be found later and $e(t)$ is measured reference error time signal given as $e(t) := r - \tilde{y}$ with r being the target output and $\tilde{y}$ the actual output. Each gain has a different purpose within the control setting, as discussed in [19]. The proportional control, k_p, is used when the action of the controller needs to be proportional to the magnitude of the error signal, $e(t)$. The integral control, k_i, is used in order for the controller to correct for any steady offset from a reference signal value. The derivative control, k_d, uses the rate of change of the error signal, $e(t)$, to increase the overall control effort.

Solving this problem in the time domain is overly complex; however the use of a Laplace transform into the frequency domain converts (5.2) into an algebraic equation, such as in [4]. As (5.2) and (5.3) are linear combinations of functions (even though those functions are not necessarily linear) and thanks to the linearity property of the Laplace transform (as described in [4]), the transform of each of these equations is equivalent to linear combination of transforms. That is, the transform of a linear combination is a linear combination of transforms. Transforming (5.2) yields

$$(-\frac{s}{A} + 1)X(s) = -\frac{B}{A}U(s)e^{-ds}. \tag{5.4}$$

Solving for $X(s)$, (5.4) is represented by

$$X(s) = \frac{ke^{-Ls}}{Ts+1}U(s), \tag{5.5}$$

with $k = -\frac{B}{A}$, $L = d$, and $T = -\frac{1}{A}$. $A < 0$, $k, T > 0$ ensures that the problem is open loop stable by the theorems set forth in [33] and can therefore be solved using the described methods in the text. $U(s)$ is found by transforming (5.3) yielding

$$U(s) = k_p E(s) + k_i E(s)\frac{1}{s} + k_d s E(s); \tag{5.6}$$

therefore the control transfer function is given by

$$C(s) = \frac{U(s)}{E(s)} = k_p + \frac{k_i}{s} + k_d s, \tag{5.7}$$

which is now an algebraic equation and not an integro-differential equation. Using the Laplace transform has also taken the delay term in (5.2) and transformed it to an exponential decay in (5.4).

5.3.2 Stabilization of PID Parameters

Following a main result in [33], we know that the range of k_p values for which the open-loop stable problem can be stabilized using a PID controller is given by the condition

$$-\frac{1}{k} < k_p < \frac{1}{k}\left[\frac{T}{L}\alpha\sin(\alpha) - \cos(\alpha)\right], \tag{5.8}$$

where α satisfies the equation

$$\tan(\alpha) = -\frac{T}{T+L}\alpha, \tag{5.9}$$

with the restriction $\alpha \in (0, \pi)$; α is found using the Bisection method in this work. These values of k_p are then used in

$$kk_p + \cos(z) - \frac{T}{L} z \sin(z) = 0, \tag{5.10}$$

where the value z is also found using the bisection method. As there is a range of possible values of k_p, it stands to reason that there are also many solutions to (5.10). These solutions, z_j, are then used in

$$\begin{aligned} m_j(z_j) &= \frac{L^2}{z_j^2} \\ b_j(z_j) &= -\frac{L}{kz_j}\left[\sin(z_j) + \frac{T}{L} z_j \cos(z_j)\right], \end{aligned} \tag{5.11}$$

with distinct solutions being found for each solution of (5.10). With these values, we now have all the necessary information to determine the conditions for the stabilizing regions k_i and k_d. For all whole number values of j where $j \in$ [1,length(k_p)], these conditions are given by

$$\begin{aligned} k_i &> 0 \\ k_d &> m_j k_i + b_j, \\ k_d &< m_{2j} k_i + b_{2j} \end{aligned} \tag{5.12}$$

The following algorithm was coded in MATLAB® to find each set of possible values and is given in [33].

1. Initialize $k_p = -\frac{1}{k}$ and $step = \frac{1}{N+1}$, where N is the desired number of points;
2. Increase k_p as follows: $k_p + step$ (this was done using a while-loop);
3. If $k_p < k_u$ then go to step 4. Else, terminate the algorithm;
4. Find the roots z_1 and z_2 of (5.10);

5. Compute the parameters m_j and b_j, $j = 1, 2$ associated with the previously found z_j by using (5.11);
6. Determine the stabilizing region in the $k_i - k_d$ space using (5.12);
7. Go to step 2;

Following these conditions creates different trapezoidal or triangular shaped planes for each value of k_p. These planes are shown in Figure 5.6 for the system under consideration here.

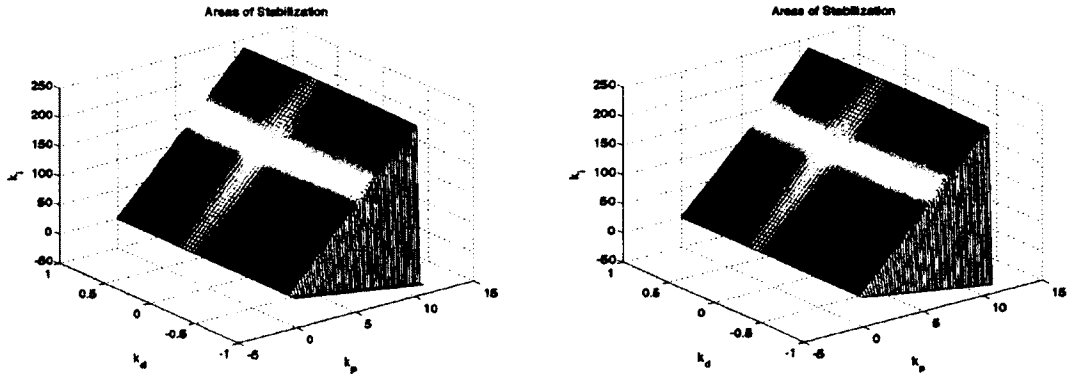

Figure 5.6: Areas of Stabilization for the 1x model (left) and 2x model (right)

5.3.3 Results Using the PID Control

Within the areas of stabilization shown in Figure 5.6, all values of k_p, k_i, and k_d will provide a solution of (5.2) and (5.3); this means that, since the parameters are real values, there are as many solutions as there are combinations of the parameters. To be certain that a solution of minimal error was found, each combination of parameters was considered and the overshoot (in regards to the target of the tracking control) was found. Also, the norm of the difference of each solution vector and the tracking target was calculated. Each solution was first found by solving (5.5) in the frequency

domain and then performing a numerical inverse Laplace transform using the code found in [3], which then provides the solution to (5.2) and (5.3) in the time domain. The overshoot, plotted against the respective function's k_i and k_p values is shown in Figure 5.7. This figure shows the wide range of overshoot values that are found when each combination of parameters is considered. The average overshoot for each model is on the magnitude of at least 10^{14} meaning that the choice of parameters is of utmost importance when using this control design.

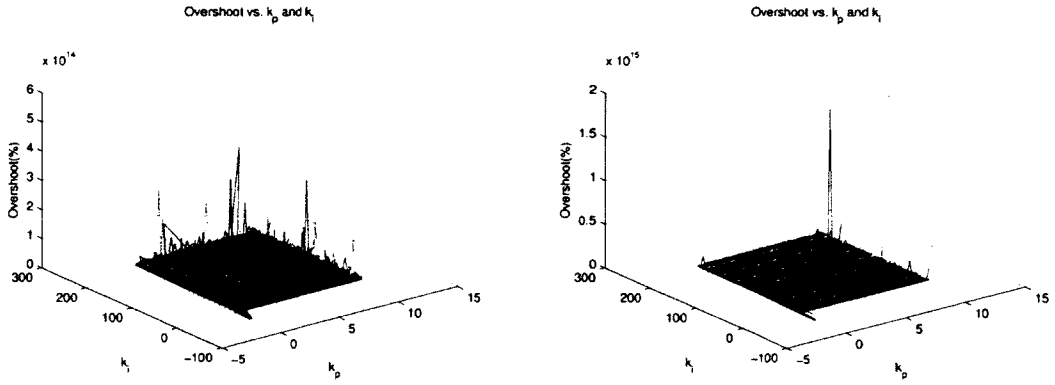

Figure 5.7: Overshoot for 1x (left) and 2x (right) models

The solution sets utilizing of k_i, k_p, and k_d that provided the lowest norm calculation were considered desirable and are plotted in Figures 5.8 and 5.9. The solution set with the lowest norm was chosen in an effort minimize the stabilizing time of the model and that with the lowest overshoot was chosen in an effort to minimize the overall required injection. The values in the solution set were then converted from OD to μL using (4.21) and plotted in Figures 5.10 and 5.11. It would also be considered appropriate to use the overshoot as the performance criteria for this controller because it is desired to limit the total injection amount while still

tracking the absorbance to a desired value and limiting the overshoot accomplishes this. However, limiting the overshoot will not necessarily lessen the stabilizing time of the model and therefore may not allow the nanoparticles to build in the bloodstream.

The plots shown in Figures 5.8 and 5.9 show that the controller tracks to the desired value within the time frame of the experiment and with the initial absorbance value of 0 OD. The initial absorbance value for this controller is set to zero in order to more closely follow the examples given in the literature. However, because the initial absorbance value will typically be zero in an experimental setting, this is an appropriate condition to follow. There is also very little oscillation in the plots shown in Figures 5.8 and 5.9 and it stabilizes to the target very quickly. With the absorbance values initially being below the target (unlike past strategies), it is likely that the level of required injection would be lower when compared to the other strategies.

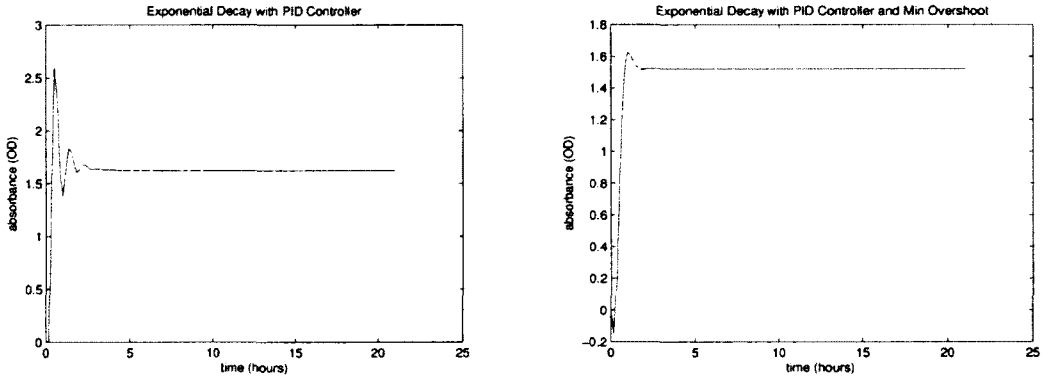

Figure 5.8: Controlled 1x with min norm (left) and with min overshoot (right) (OD), varied axes

While the models that give the minimum norm calculation do not necessarily show a faster stabilizing time than those with the minimum overshoot, they do show quick stabilizing times and are an appropriate way to guarantee a minimal (if not

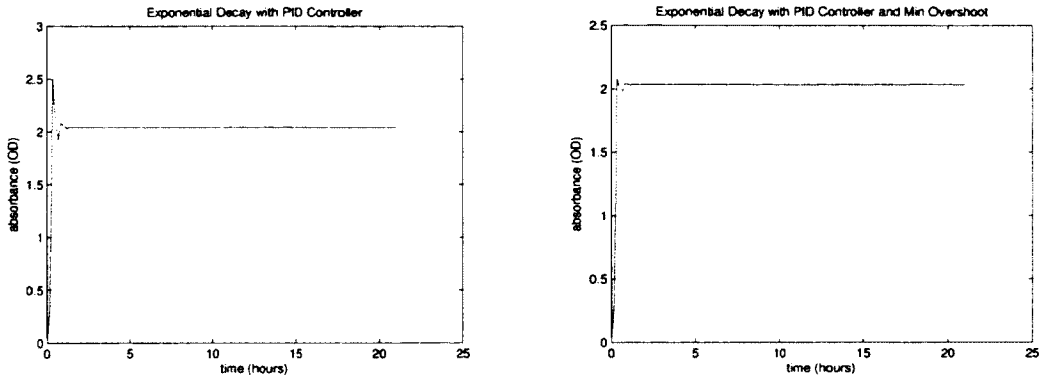

Figure 5.9: Controlled 2x with min norm (left) and with min overshoot (right) (OD), varied axes

the most minimal) stabilizing time when used with future models. Calculating the injection over time for these models was a two part process: the first to account for the injections made before the model stabilizes and the second is for the time following the stabilization of the model (when measured in OD). For the first portion of the calculation, the injection was found using the conversion given by (4.21) with the absorbance value at each time point. The injection amount necessary to build to the absorbance at any one time point is then equal to difference between μL at that time point and the μL at the preceding time point. Once the controlled model stabilizes to the tracking target, this method to find the injection amount is no longer useful as the difference in μL between one time point and the next would be very close to zero and, therefore, not an accurate description of the nanoparticles needed to maintain the absorbance at a particular value. For this reason, once the model reaches the point of stabilization, the amount of nanoparticles needed is found in the same way as it is for the LQR controller. That is, we are basically finding the area between the μL curves for the controlled and uncontrolled models, where the uncontrolled

model is the exponential decay function given by (2.4) with an initial value equal to the tracking target and a horizontal translation to account for the time taken for the model to stabilize to that target. The values found are shown in Figures 5.10 and 5.11 and the total injection amounts are given in Table 5.3.

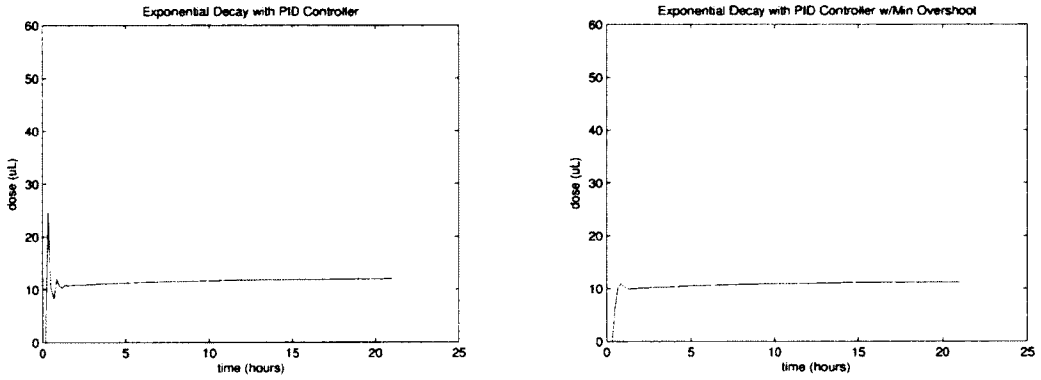

Figure 5.10: Controlled 1x with min norm (left) and with min overshoot (right) (μL)

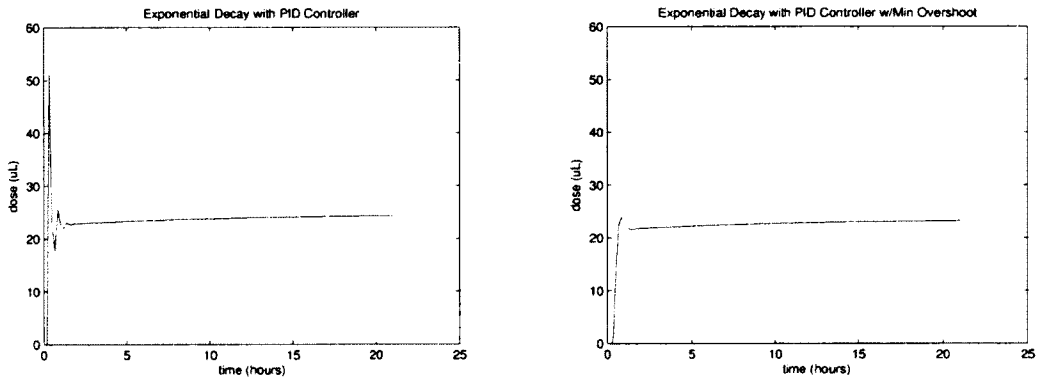

Figure 5.11: Controlled 2x with min norm (left) and with min overshoot (right) (μL)

5.4 Comparison of the Methods of Control

Aside from simply comparing the plots produced by each method of control, the only way to properly compare the models is to compare the total error for each model (which is found using the Total Least Squares method in [30]) along with the required overall dose (in μL) for each model. Each of those values was found and given in Tables 5.3 and 5.4, respectively. Judging by the error alone, it would seem

Table 5.3: Total Dose of Each Control Strategy

	1x	2x	half 1x	half 2x
initial absorbance (OD)	3.2475	4.1573	1.6238	2.0789
target absorbance (OD)	1.6238	2.0789	1.6238	2.0789
LQR control total dose (μL)	234.64	1080.92	65.25	299.1
Dirac delta total dose (μL)	127.3	235.33	66.07	115.08
PID control(w/0 initial OD)		w/min norm	242.58	498.25
total dose (μL)	*	w/min overshoot	222.80	467.31

Table 5.4: Total Error According to Initial Absorbance

Initial / Target Absorbance (OD)	No Control	PID Control w/min overshoot	PID Control w/min norm
0 / 1.6238	*	2.4529	0.2957
0 / 2.0789	*	0.3820	0.5666
		LQR Control	Dirac delta
3.2475 / 1.6238	430.81	178.47	285.73
4.1573 / 2.0789	472.66	539.72	432.52
1.6238 / 1.6238	572.93	140.89	39.44
2.0789 / 2.0789	695.07	26.53	105.9

that the PID control (whether by using the minimum overshoot or the minimum norm) is the most efficient. However, because of the methods involved in stabilizing

the PID controller, it requires several minutes to hours to run; as opposed to the other strategies which require seconds to minutes. The PID controller also requires a rather high total dose which is expected as it is the only method of control analyzed that held the absorbance level to the desired target. This is not ideal when future work is considered as we would want to apply the controller during a real-time experiment. With this being said, it would appear using Dirac delta functions as the method of control is the most efficient as it provides low error and a low total injection. This method is also able to keep the absorbance level close to the target for the bulk of the experiment (as can be seen in Figures 5.4 and 5.5) and should be easily replicable in an experimental setting with some animals when a continuous infusion is not possible. When a continuous infusion is a possibility, the LQR control strategy is an efficient choice as well.

CHAPTER 6

CONCLUSIONS AND FUTURE WORK

6.1 Summary and Conclusions

In this work, several different models are presented to represent the nanoparticle concentration in the bloodstream over time via absorbance measurements. The algebraic model is described in (2.3) and plotted for the particular mouse in Figure 2.1. Though it was a good starting point, this model was found to have a low R-squared value for each mouse modeled. It was determined that, overall, this model skewed the time of maximum absorbance to a later time point; it also tended to yield low maximum absorbance predictions. For those reasons, a new model was used.

The absolute value model described in (2.5) and plotted for the particular mouse in Figure 2.3 has shown to improve upon the issues found with the rational model. As the absolute value model is capable of a much faster rise in the dependant variable, the skew of the time of maximum absorbance shown in Figure 2.1 was better accounted. This model also showed better overall predictions of the maximum absorbance. However, much like the algebraic model, this model was unable to account for the false 'peak' in nanoparticle uptake; this refers to the high maximum absorbance that quickly drops off, most likely due to poor coating of some of the

injected nanoparticles. As neither the algebraic nor the rational model were able to account for this perceived error, the exponential model was created.

Figure 2.2 plots (2.4) for the same particular mouse of the above two models. This exponential model not only accounts for the false 'peak' of nanoparticles, but also gives a more 'close up' view of the retention phase of the experiment; this is of particular interest for the control effort portion of this research. As the goal of the control effort for the current model is to maximize the retention of nanoparticles in the bloodstream, the control effort is focused on the exponential model only. Using this model and the injection profiles described in (2.6), the piecewise model was found and further used for the control effort described in Chapter 4.

Upon running the statistical tests it was found that the data within the 1x and 2x models were statistically similar and, therefore, we were able to create average models, or 'Master Mice', for the 1x and 2x best fits of each model presented in Chapter 2. Confidence and prediction intervals were then found for each 'Master Mouse' for each model. These plots are now theoretically able to be used in real time in order to see adverse reactions and other possible issues during the experiment.

Several different control strategies were analyzed in Chapters 4 and 5. Initially, in Chapter 4 a tracking LQR controller with a DDE is used assuming the same initial injection as is used experimentally. Then, in Chapter 5 this same controller is used with different initial injections for the purpose of limiting the overall amount of nanoparticles required for the entire experiment. Then, the use of Dirac delta functions as a control strategy was analyzed to observe if a discrete number of injections would be at least as effective as the continuous injection in the LQR

controller. Finally, as it is a more commonly used controller in the engineering or industrial settings, a tracking PID controller was used on the DDE. Each strategy was found to be efficient and proficient at tracking to a desired target (in this case, tracking to a desired absorbtion). The total amount of required nanoparticles (in μL) was found along with the error for each model and these values are given in Tables 5.1 and 5.4, respectively. Each strategy required a different amount of nanoparticles to reach the desired target. However, as the error and oscillation of the different solutions also varied, it is not entirely clear which strategy is the most efficient for experimental use.

While each method was shown to be effective, the Dirac delta functions appeared to be the most efficient as it yielded low error with minimal total injection and short run time. This control method was also able to keep the absorbance value very close to the target for the majority of the length of the experiment.

6.2 Discussion and Future Work

Each control effort, with the possible exception of the PID control, applied to the exponential decay model shown runs within the time frame for which it could be used in an experimental setting. Currently, the confidence and prediction intervals described in Chapter 3 are in the beginning stage of being implemented for use in real time during the run of the experiments. With the models being created in real time it would be possible to see adverse reactions as they are happening and thus better treat the patient. Once this is accomplished, it is the goal to implement a control strategy in an experimental setting as well. Each controller shows a different method

with different results to consider so the choice of control strategies to implement will most likely depend on the specific needs of the individual patient.

These models only show a single biological compartment (that is, they model the entire body at one time). Ideally, several different compartments will be added, such as the tumor, reticulo endothelial system, and bloodstream (similar to the models discussed in [17]). Currently the experimental data does not provide the necessary information to show a multi-compartment model. The addition of these compartments will provide much better insight into where the nanoparticles are actually accumulating once they enter the body. The additional models will also provide more opportunities for control design strategies to be applied. It would be of specific interest to minimize the nanoparticle elimination by the reticulo endothelial system and to maximize the nanoparticle uptake in the tumor. Ideally, these methods can also be used with other treatment strategies than the nanoparticle dosages if enough data were provided for those methods.

BIBLIOGRAPHY

[1] http://research.latech.edu/directory/project/211, 2010.

[2] http://www.oswego.edu/ srp/stats/pi.htm, 2011.

[3] J. Abate and W. Whitt. A unified framework for numerically inverting laplace transforms. *INFORMS Journal of Computing*, 18(4):408, 2006.

[4] D. G. Zill ad M. R. Cullen. *Differential Equations with Boundary-Value Problems.* Thompson Brooks/Cole, 6 edition, 2005.

[5] P. Arora and P.N. Tandon. Mathematical models for drug delivery to chronic patients. *Applied Mathematical Modeling*, 33:692–705, 2009.

[6] H. T. Banks and J. A. Burns. Hereditary control problems: numerical methods based on averaging approximations. *SIAM Journal on Control and Optimization*, 16:169–208, 1978.

[7] M. Basin and J. Rodriguez-Gonzalez. A closed-form optimal control for linear systems with equal state and input delays. *Automatica*, 41:915–920, 2005.

[8] A. Bensoussan, G. Da Prato, M. Delfour, and S. Mitter. *Representation and Control of Infinite Dimensional Systems, Volumes I and II.* Birkhauser, Boston, 1992.

[9] F. Billy, B. Ribba, O. Saut, H. Morre-Trouihet, T. Colin, D. Bresch, J. Boissel, E. Grenier, and J. Flandrois. A pharmacologically-based multiscale mathematical model of angiogenesis and its use in investigating the efficacy of a new cancer treatment strategy.

[10] F. Castiglione and B. Piccoli. Cancer immunotherapy, mathematical modeling and optimal control. *Jounal of Theoretical Biology*, 247:723–732, 2007.

[11] C. Collins, K.R. Fister, B. Key, and M. Williams. Blasting neuroblastoma using optimal control of chemotherapy. *Mathematical Biosciences and Engineering*, 6:451–467, 2009.

[12] S. Dash, P.N. Murthy, L. Nath, and P. Chowdhury. Kinetic modeling on drug release from controlled drug delivery systems. *Acta Poloniae Pharmaceutica - Drug Research*, 67(3):217–223, 2010.

[13] M. C. Delfour and S. K. Mitter. Controllability, observability and optimal feedback control of hereditary differential systems. *SIAM Journal on Control and Optimization*, 10:298–328, 1972.

[14] C. Deroulers, M. Aubert, M. Badoual, and B. Grammaticos. 2009.

[15] A. d'Onfrio. Metamodeling tumor-immune system interaction, tumor evasion and immunotherapy. *Mathematical and Computer Modeling*, 47:614–637, 2008.

[16] P. Dorato, C. Abdallah, and V. Cerone. *Linear-Quadratic Control, An Introduction.* Prentice Hall, Englewood Cliffs, 1995.

[17] A. Osol et. al, editor. *Remington's pharmaceutical sciences.* Mack Publishing Company, 15 edition, 1975.

[18] W.D. James, L.R. Hirsch, J.L. West, P.D. O'Neal, and J.D. Payne. Application of INAA to the build-up and clearance of gold nanoshells in clinical studies in mice. *Journal of Radionalytical and Nuclear Chemistry*, 271(2):455–459, 2007.

[19] M. A. Johnson and M. H. Moradi, editors. *PID Control: New Identification and Design Methods.* Springer, 2005.

[20] S. Keiding. Hepatic clearance and liver blood flow. *Journal of Hepatology*, 4:393–398, 1987.

[21] M. Legua, I. Morales, and L.M. Sánchez Ruiz. Dirac delta in matlab.

[22] J. Li, G. L. Dobson, M. P. Marietta, G. R. Rhodes, and I. J. Hidalgo. *In vivo* determination of drug kinetic linearity and individual organ elimination by the accelerated infusion technique. *Journal of Pharmacological and Toxicological Methods*, 37:47–53, 1997.

[23] D. Mackenzie. Mathematical modeling and cancer. *SIAM News*, 37(1), 2004.

[24] P.A. Mackowiak, S.S. Wasserman, and M.M. Levine. A critical appraisal of 98.6 degrees f, the upper limit of the normal body temperature, and other legacies of Carl Reinhold August Wunderlich. *Journal of the American Medical Association*, 268:1578–1580, 1992.

[25] M. Malek-Zavarei and M Jamshidi. *Time-Delay Systems: Analysis, Optimization and Applications.* Elsevier Science Ltd, North-Holland Systems and Control Series, 1987.

[26] G. J. Michalak, A. Anderson, and D. P. O'Neal. Feasibility of using a two-wavelength photometer to estimate the concentration of circulating near-infrared extinguishing nanoparticles. *Journal of Biomedical Nanotechnology*, 6(1):1–10, 2010.

[27] G. J. Michalak, G. P. Goodrich, J. A. Schwartz, W. D. James, and D. P. O'Neal. Murine photoplethysmography for *in vivo* estimation of vascular gold nanoshell concentration. *Journal of Biomedical Optics*, 15, July/August 2010.

[28] G. J. Michalak, J. A. Schwartz, G. P. Goodrich, and D. P. O'Neal. Three-wavelength murine photoplethysmography for estimation of vascular gold nanorod concentration. *Optics Express*, 18(25):26535–26549, 2010.

[29] S. Nie. Understanding and overcoming major barriers in cancer nanomedicine. *Nanomedicine*, 5:523–528, June 2010.

[30] I. Patráš and D. Bednárovaá. *Acta Montanistica Slovaca*, 15(2):158–170, 2010.

[31] M. Paun. Stat 680: Biostatistics. 2011.

[32] X. Peng. Targeted delivery of cisplatin to lung cancer using [s]cfvegfr-heparin-cispaltin nanoparticles. *ACS Bank*, 5(12), 2011.

[33] G. J. Silva, A. D., and S.P. Bhattacharyya. *PID Controllers for Time-Delay Systems*. Birkhäuser, 2005.

[34] M. Sipics. Mathematics meets oncology and immunology. *SIAM News*, 42(8):1–4, 2008.

[35] M. A. Soliman and W. H. Ray. Optimal control of multivariable systems with pure time delays. *Automatica*, 7:681–689, 1971.

[36] M. A. Soliman and W. H. Ray. Optimal feedback control for linear-quadratic systems having time delays. *International Journal of Control*, 15:609–627, 1972.

[37] A. Świerniak, U. Ledzewicz, and H. Schättler. Optimal control for a class of compartmental models in cancer chemotherapy. *Int. J. Appl. Math. Comput. Sci.*, 13(3):357–368, 2003.

[38] J.A. Tichý, M. Loučka, and Z.M. Trefný. The new clearance method for hepatic diagnostics. *Prague Medical Report*, 106(3):229–242, 2005.

[39] G. Xu and H. L. McLeod. Strategies for enzyme/prodrug cancer therapy. *Clinical Cancer Research*, 7:3314–3324, 2001.